1 **Competition between myosin II and β_H-Spectrin regulates cytoskeletal tension**

2 Consuelo Ibar[1], Krishna Chinthalapudi[2], Sarah M. Heissler[2] and Kenneth D. Irvine[1]*

3 [1]Waksman Institute and Department of Molecular Biology and Biochemistry, Rutgers

4 University, Piscataway NJ 08854 USA

5 [2]Department of Physiology and Cell Biology, Dorothy M. Davis Heart and Lung Research

6 Institute, The Ohio State University College of Medicine, Columbus, Ohio, USA

7 *Corresponding author: irvine@waksman.rutgers.edu

ABSTRACT

Spectrins are membrane cytoskeletal proteins generally thought to function as heterotetramers comprising two α-spectrins and two β-spectrins. They influence cell shape and Hippo signaling, but the mechanism by which they influence Hippo signaling has remained unclear. We have investigated the role and regulation of the *Drosophila* β-heavy Spectrin (β_H-Spectrin, encoded by the *karst* gene) in wing imaginal discs. Our results establish that β_H-Spectrin regulates Hippo signaling through the Jub biomechanical pathway due to its influence on cytoskeletal tension. While we find that α-Spectrin also regulates Hippo signaling through Jub, unexpectedly, we find that β_H-Spectrin localizes and functions independently of α-Spectrin. Instead, β_H-Spectrin co-localizes with and reciprocally regulates and is regulated by myosin. In vivo and in vitro experiments support a model in which β_H-Spectrin and myosin directly compete for binding to apical F-actin. This competition can explain the influence of β_H-Spectrin on cytoskeletal tension and myosin accumulation. It also provides new insight into how β_H-Spectrin participates in ratcheting mechanisms associated with cell shape change.

INTRODUCTION

The spectrin cytoskeleton has been described as a lattice of cross-linked, spring-like proteins that provide structural support to cells (Liem, 2016; Machnicka et al., 2014). Spectrins were first discovered and characterized in red blood cells but are expressed in many cell types. Spectrins can bind to cell membranes and F-actin, linking them together. They are generally thought to act as heterotetramers, composed of two α subunits and two β subunits. *Drosophila* has one α-spectrin (α-Spec) and two β-spectrins: β-Spectrin (β-Spec) and β-Heavy-Spectrin (β_H-Spec, encoded by *karst* (*kst*)), which could potentially generate two distinct spectrin heterotetramers: $(\alpha\beta)_2$ and $(\alpha\beta_H)_2$. β-Spec and β_H-Spec interact with F-actin through their N-terminal domains, which contain two actin-binding calponin-homology (CH) domains, connecting the spectrin cytoskeleton to the actin cytoskeleton (Liem, 2016). In *Drosophila* epithelia, it has been reported that β-Spec localizes to the lateral sides of cells, β_H-Spec localizes to the apical sides of cells, and α-Spec localizes both laterally and apically, leading to inferences that spectrin exists as lateral $(\alpha\beta)_2$ tetramers and apical $(\alpha\beta_H)_2$ tetramers (Dubreuil et al., 1997; Lee et al., 1997; Thomas et al., 1998; Zarnescu and Thomas, 1999). Despite common assumptions that spectrins act as tetramers, there is some evidence that alternative arrangements may exist. In *Drosophila* ovarian follicle cells, the absence of α-Spec diminishes the recruitment of β_H-Spec to the apical domain, but it does not affect the recruitment of β-Spec to the lateral domain (Lee et al., 1997). Examination in *Drosophila* of a mutant form of α-Spec that, based on in vitro studies, is unable to bind β-spec and compromised in its ability to bind β_H-Spec, revealed that it could nonetheless rescue the lethality of an *α-Spec* mutant (Khanna et al., 2015). Experiments done with a mammalian homolog of β_H-Spec, βV-Spec, showed that it can

44 homodimerize through its C-terminal region, raising the possibility that βV-Spec might be able
45 to cross-link F-actin by itself (Papal et al., 2013).

46 Several studies have reported that spectrins also regulate Hippo signaling, with effects on
47 readouts of Hippo signaling reported in *Drosophila* imaginal discs and ovarian follicles, as well
48 as in cultured mammalian cells (Deng et al., 2015; Deng et al., 2020; Fletcher et al., 2015; Wong
49 et al., 2015). Hippo signaling is a signal transduction network that responds to diverse upstream
50 inputs, including the cytoskeleton and cells' physical environment (Misra and Irvine, 2018;
51 Zheng and Pan, 2019). Hippo signaling modulates cell proliferation and fate, largely through the
52 regulation of Yap family transcriptional co-activator proteins (Yorkie, Yki, in *Drosophila*, YAP1
53 and TAZ in humans). Yki is primarily regulated through phosphorylation by the kinase Warts
54 (Wts), which promotes the cytoplasmic localization of Yki. Various potential mechanisms for
55 biomechanical regulation of Yki/Yap activity have been described, but the best-characterized
56 mechanism in *Drosophila* is the Jub biomechanical pathway. This involves tension-dependent
57 recruitment of an Ajuba LIM protein (Jub in *Drosophila*, LIMD1 in mammals) to α-catenin at
58 adherens junctions (AJ) (Alegot et al., 2019; Ibar et al., 2018; Rauskolb et al., 2022; Rauskolb et
59 al., 2014; Sarpal et al., 2019; Sun et al., 2015). Jub then recruits and inhibits Wts, resulting in
60 increased Yki activity.

61 Studies of the influence of spectrins on Hippo signaling have suggested different
62 mechanisms by which this might occur (Deng et al., 2015; Deng et al., 2020; Fletcher et al.,
63 2015; Wong et al., 2015). Fletcher et al. (2015), focusing on β_H-Spec, suggested that the spectrin
64 cytoskeleton influences the membrane density, and thereby the activation state, of upstream
65 regulators of Hippo signaling. Wong et al. (2015), focusing on β-Spec, suggested that spectrins

66 might influence Hippo signaling by modulating levels of F-actin; increased levels of F-actin have
67 been reported in other studies to be associated with increased Yki/Yap activity (Aragona et al.,
68 2013; Fernandez et al., 2011; Sansores-Garcia et al., 2011). Deng et al. (2015), focusing on α-
69 Spec, reported that spectrins regulate levels of phosphorylated myosin light chain (required for
70 myosin activation) but surprisingly did not affect levels of myosin or recruitment of Jub, leading
71 them to infer that spectrins can act through a novel tension-dependent but Jub-independent
72 pathway. These same authors later reported that in the pupal eye, spectrins can act through Jub,
73 while suggesting that the action of spectrins in the pupal eye differs from their action in the wing
74 disc (Deng et al., 2015; Deng et al., 2020).

75 The disparate models for how spectrins influence Hippo signaling have led to confusion
76 over whether a distinct spectrin-based mechanism exists for the mechanical regulation of Hippo
77 signaling. We were particularly interested in investigating claims that spectrins could alter
78 cytoskeletal tension in wing discs without affecting Jub localization or levels of myosin. Our
79 results reveal that both β_H-Spec and α-Spec influence Jub recruitment to AJ, and their effects on
80 Yki activity depend upon Jub. Together, these observations argue that spectrins influence Hippo
81 signaling through the Jub biomechanical pathway. Unexpectedly, our investigations also reveal
82 that β_H-Spec and α-Spec act separately in wing discs - they do not co-localize, nor do they
83 influence each other's localization. These observations argue that β_H-Spec does not act as part of
84 an $(\alpha\beta_H)_2$ tetramer in the wing disc but rather exerts its functions independently of α-Spec.
85 Finally, we establish that β_H-Spec and myosin reciprocally antagonize each other's apical
86 localization in wing discs - myosin inhibits β_H-Spec, and β_H-Spec inhibits myosin. We further
87 show that myosin can compete with β_H-Spec for binding to F-actin in vitro. Together with
88 structural modeling, our observations argue that β_H-Spec and myosin compete with each other

89 for binding to F-actin in vivo. This competition could explain how β_H-Spec influences myosin
90 activity and further suggests a simple mechanism for the contribution of β_H-Spec to ratcheting
91 processes that alter cell shape via actomyosin contractility.
92
93 **RESULTS**
94 **β_H-Spectrin regulates myosin activity and levels in wing imaginal discs**
95 Prior studies have reported that mutation or RNAi-mediated knockdown of spectrins in
96 wing and eye imaginal discs increased myosin activity, as visualized by staining for myosin light
97 chain phosphorylated at activation sites (pMLC) (Deng et al., 2015; Forest et al., 2018).
98 Surprisingly, it was also reported that levels of GFP-tagged myosin light chain (encoded in
99 *Drosophila* by spaghetti squash, Sqh:GFP) or F-actin were nonetheless unaffected (Deng et al.,
100 2015), whereas changes in myosin activity generally correlate with changes in myosin
101 accumulation (Fernandez-Gonzalez et al., 2009; Noll et al., 2017). To re-examine this, we
102 analyzed wing imaginal discs in which the apical, β_H-Spec *kst* was knocked down in posterior
103 wing cells by expressing UAS-RNAi lines under *en-Gal4* control (RNAi validation is presented
104 in Figure 1 – figure supplement 1). This approach leaves unaffected anterior wing disc cells as an
105 internal control. These experiments typically also include a neutral transgene expressed under
106 en-Gal4 control to mark posterior cells (e.g. UAS-RFP) and a transgene expressing Dicer2
107 (Dcr2) to increase the efficacy of RNAi (Dietzl et al., 2007). This increased apical pMLC in
108 posterior cells, where levels of β_H-Spec were reduced (Figure 1- figure supplement 2B and D),
109 consistent with previous reports (Deng et al., 2015; Forest et al., 2018). A difference in
110 junctional tension between anterior (control) cells and posterior (β_H-Spec RNAi) cells in our
111 experiments was confirmed by measuring the recoil velocity of cell junctions after laser cutting,

112 which demonstrated an increased tension in the β_H-Spec depleted sides (Figure 1G). To examine
113 myosin protein levels, we employed the myosin light chain GFP fusion Sqh:GFP. We found that
114 depletion of β_H-Spec led to increased levels of junctional myosin (Figure 1B). To quantify these
115 effects on Sqh:GFP levels, we made maps of Sqh:GFP intensity normalized against E-cad
116 intensity. These are displayed on a red (high) to blue (low) heat map (Pan et al., 2018) and we
117 also used this analysis to calculate the ratio of intensities of the anterior (control) versus posterior
118 (experimental) compartments (Alegot et al., 2019) (Figure 1D-E, H-I). This was further
119 confirmed by using a distinct β_H-Spec RNAi line (*UAS-kstRNAi*^{HMS00882}), which similarly
120 increased myosin levels (Figure 1- figure supplement 2E).

121 As earlier studies reporting no effect on myosin levels focused on mutation or
122 knockdown of α-Spec (Deng et al., 2015), we considered the possibility that knockdown of α-
123 and β_H-Spec might differ in their effects on apical myosin accumulation. However, we found that
124 knockdown of α-Spec also caused an increased accumulation of apical myosin, as well as pMLC
125 and junctional tension, similar to the effects of β_H-Spec knockdown (Figure 1C, F, H, I; Figure 1-
126 figure supplement 2C and D). α-Spec and β_H-Spec knockdown differed though in that the
127 thickness of the wing disc epithelium was reduced by α-Spec knockdown, but not by β_H-Spec
128 knockdown (Figure 1- figure supplement 3), indicating that even though α-Spec and β_H-Spec
129 have similar effects on junctional myosin, their roles in wing disc cells differ. Studies in pupal
130 eyes identified a role for α-Spec in attaching F-actin to membranes that was associated with
131 maintaining proper cortical tension and cell shape (Deng et al., 2020); we think the reduced
132 thickness of the epithelium is a reflection of this role in wing discs. That is, reduced stiffness of
133 the lateral sides of cells when α-Spec is removed may allow cells to expand laterally, and
134 through conservation of volume, simultaneously shorten along the apical-basal axis.

135

136 **β_H-Spec regulates Hippo signaling through Jub**

137 It was previously argued that spectrins do not influence Hippo signaling through the Jub
138 biomechanical pathway in wing discs, in part based on an apparent lack of effect of *α-Spec*
139 mutation or depletion on Jub localization (Deng et al., 2015). However, multiple studies have
140 consistently observed that Jub localization increases when tension at AJ is increased (Forest et
141 al., 2018; Pan et al., 2018; Rauskolb et al., 2019; Rauskolb et al., 2014; Razzell et al., 2018).
142 Thus, we examined Jub localization under conditions of β_H-Spec depletion. In wing imaginal
143 discs, Jub accumulates in puncta that often occur near intercellular vertices, together with a
144 lower-level, more even accumulation along the cell-cell junctions (Figure 2A and Figure 2–
145 figure supplement 1B). Jub is recruited by a tension-dependent conformational change of α-
146 catenin, and Jub puncta are increased when cytoskeletal tension is higher. Consistent with this,
147 examination of Jub:GFP confirmed that the increased junctional tension and myosin activity
148 caused by β_H-Spec depletion is associated with increased junctional recruitment of Jub (Figure
149 2B, E, G-H and Figure 2 -figure supplement 1C).

150 To assess the functional significance of increased Jub localization to AJ under β_H-Spec
151 knockdown conditions, we assayed the ability of RNAi-mediated *jub* knockdown to suppress β_H-
152 Spec (kst) RNAi phenotypes. Knockdown of β_H-Spec throughout the developing wing under
153 *nub-Gal4* control increases wing size (wings were 116% and 119% of *nub-Gal4 UAS-dcr2*
154 control size for the two different UAS-RNAi lines used) (Figure 3A, C-D and K) (Deng et al.,
155 2015; Fletcher et al., 2015). Knockdown of *jub* leads to smaller wings (Das Thakur et al., 2010;
156 Rauskolb et al., 2011). In animals with simultaneous RNAi knockdown of *jub* and *kst,* wing size
157 is similar to that of *jub* RNAi wings (Figure 3B, E-F and K). The epistasis of *jub* to *kst* is

158 consistent with the hypothesis that β_H-Spec regulates wing size through its tension-dependent
159 regulation of Jub. To further illustrate this, we reduced tension in wing discs with β_H-Spec
160 knockdown by simultaneous RNAi knockdown of *Rho kinase (Rok)* (Rauskolb et al., 2014;
161 Winter et al., 2001). This reduced wing size and junctional Jub localization similar to that
162 observed in control wing discs with *Rok* knockdown (Figure 3-figure supplement 1) (Rauskolb et
163 al., 2014).

164 To confirm that the relationship between Jub and β_H-Spec revealed by analysis of adult
165 wing size corresponds to changes in Hippo pathway activity, we analyzed the expression of a
166 transcriptional reporter of *expanded (ex)*, *ex-lacZ*, which is a direct target of Yki (Hamaratoglu et
167 al., 2006). Knockdown of β_H-Spec in posterior compartments through the expression of UAS-*kst*
168 RNAi under *en-Gal4* control caused a mild increase in *ex-lacZ* expression compared to the
169 anterior compartment and to control posterior compartments (Figure 3L,M) (Fletcher et al.,
170 2015). Knockdown of *jub* reduces *ex-lacZ* expression (Das Thakur et al., 2010; Rauskolb et al.,
171 2011). Simultaneous RNAi knockdown of *jub* and *kst* reduced *ex-lacZ* expression, similar to that
172 in *jub* RNAi cells (Figure 3N,O). The suppression of the influence of *kst* on Hippo signaling is
173 again consistent with the inference that β_H-Spec regulates Hippo signaling through the Jub
174 biomechanical pathway.

175 As claims that spectrins act independently of Jub in wing discs were based primarily on
176 analysis of α-Spec, we also examined the effect of α-Spec knockdown on Jub levels. When α-
177 Spec was knocked down in posterior cells by *en-Gal4* driven RNAi, we observed that
178 recruitment of Jub to cell junctions was increased (Figure 2C, F-H). Moreover, as for β_H-Spec,
179 we found that the increased wing size and *ex-lacZ* expression caused by knockdown of α-Spec
180 were suppressed by knockdown of *jub* (Figure 3G, H, K and P,Q). Thus, as for β_H-Spec, and as

181 suggested for pupal eyes (Deng et al., 2020), our observations imply that α-Spec also regulates
182 Hippo signaling through Jub in wing discs.
183
184 **β_H-Spec localizes independently from α-Spec in wing disc cells**
185 Prior studies of spectrin function in imaginal discs have assumed that they function as
186 heterotetramers, with an apical complex composed of $(\alpha\beta_H)_2$ subunits and a lateral complex
187 composed of $(\alpha\beta)_2$ subunits (Deng et al., 2015; Deng et al., 2020; Fletcher et al., 2015; Thomas
188 et al., 1998), as was originally suggested for ovarian follicle cells (Lee et al., 1997). However,
189 our examination of spectrin localization in wing imaginal discs suggested that the apical-most
190 distributions of α-Spec and β_H-Spec differ. To directly compare them, we used an antibody
191 against α-Spec (Dubreuil et al., 1987) and a fully functional genomic YFP-trap of β_H-Spec
192 (Kst:YFP) (Lye et al., 2014). β_H-Spec is localized, as reported previously, at the apicobasal level
193 of the adherens junction in wing discs (Fletcher et al., 2015; Forest et al., 2018) (Figure 4A, C).
194 Conversely, α-Spec is enriched in a sub-apical region just below this, with slightly lower levels
195 extending all along the lateral membrane (Figure 4B, C). Only very low levels of α-Spec are
196 detected in the apical plane where β_H-Spec is detected, and their distributions in this plane appear
197 to differ (Figure 4A).
198 To confirm that β_H-Spec and α-Spec localize independently of each other in wing discs,
199 we examined the consequences of depleting α-Spec, β-Spec, or β_H-Spec on each other's
200 localization. For this, we used *en-Gal4* driven UAS-RNAi lines to knockdown one of the
201 spectrin proteins, and then examined whether the localization of the others was affected. These
202 experiments revealed, as expected, that β-Spec is not required for β_H-Spec localization (Figure
203 5B), but it does strongly reduce α-Spec localization (Figure 5E). α-Spec is not required for β_H-

204 Spec localization (Figure 5A) but its knockdown slightly reduces β-Spec localization (Figure
205 5D). Finally, β_H-Spec depletion does not affect α-Spec localization (Figure 5C). These
206 observations suggest that while α-Spec needs β-Spec to localize to lateral membranes, the
207 localization of β_H-Spec and α-Spec are functionally independent. To further examine the
208 relationship between spectrins, we performed proximity ligation assays using antibodies against
209 α-Spec and GFP. A PLA signal consistent with close association of α-Spec and β-Spec was
210 observed in wing discs expressing GFP-tagged β-Spec (Fig. 4E). Conversely, no significant PLA
211 signal was detected in wing discs expressing GFP-tagged β_H-Spec, implying that α-Spec and β_H-
212 Spec are not closely associated in wing discs (Figure 4D). Together with the distinct localization
213 of these proteins revealed by imaging, these observations argue against the existence of $(\alpha\beta_H)_2$
214 complexes in wing imaginal discs.
215

216 **β_H-Spec and apical myosin antagonize each others' localization to apical F-actin**

217 The discovery that β_H-Spec and α-Spec localize independently led us to consider what
218 factors might influence the apical localization of β_H-Spec. Intriguingly, the distribution of β_H-
219 Spec in wing disc cells appears very similar to the apical distribution of F-actin and myosin, and
220 similarities between the localization of β_H-Spec and myosin in *Drosophila* embryos have been
221 noted previously (Krueger et al., 2020; Thomas and Kiehart, 1994). To determine whether
222 myosin and β_H-Spec colocalize in wing discs, we imaged discs expressing GFP-tagged β_H-Spec
223 (Kst:GFP) and mCherry-tagged myosin light chain (sqh-Sqh:mCherry). This revealed extensive
224 co-localization between these proteins in the apical region of wing disc epithelial cells (Figure
225 6A, B). Quantitation of these images yielded a Pearson's Correlation Coefficient score of 0.636.
226 For comparison, the Pearson's Correlation Coefficient score between Kst:YFP and α-Spec

227 (Figure 4A) was 0.18. Both Kst:GFP and Sqh:mCherry also colocalized with F-actin, with
228 Pearson's Correlation Coefficient scores of 0.641 and 0.612, respectively.

229 The extensive co-localization of β_H-Spec and myosin prompted us to investigate the
230 functional relationship between them further. As noted above, reduction of β_H-Spec leads to
231 increased apical myosin levels and activity. To investigate whether myosin reciprocally regulates
232 β_H-Spec, we expressed transgenes that modulate actomyosin contractility. RNAi-mediated
233 knockdown of Rok reduces myosin activity by reducing phosphorylation of myosin light chain
234 (Winter et al., 2001). In wing discs, knockdown of *Rok* is also associated with reduced
235 recruitment of myosin to apical junctions and reduced junctional tension (Rauskolb et al., 2014)
236 (Figure 6 – figure supplement 1C), consistent with the generally positive correlation between
237 myosin activity and co-localization with F-actin (Fernandez-Gonzalez et al., 2009; Noll et al.,
238 2017). Conversely, examination of β_H-Spec in wing disc cells expressing *Rok* RNAi revealed
239 increased levels of β_H-Spec along apical junctions (Figure 6D). To increase myosin activity, we
240 expressed a constitutively activated, phosphomimetic form of myosin light chain, Sqh^{EE} (Winter
241 et al., 2001). This increases the recruitment of myosin to AJ and increases junctional tension
242 (Rauskolb et al., 2014) (Figure 6 – figure supplement 1D), but decreases the recruitment of β_H-
243 Spec to AJ, and a portion of β_H-Spec instead appears in apical vesicles (Figure 6E,F). To
244 quantify these effects on β_H-Spec levels, we made maps of β_H-Spec intensity normalized against
245 E-cad intensity, displayed on a red (high) to blue (low) heat map. Calculation of the ratio of
246 intensities of the anterior (control) versus posterior (experimental) compartments further
247 confirmed our observation that myosin antagonizes localization of β_H-Spec to AJ (Figure 6G-J).
248 Thus, β_H-Spec and myosin II localization to AJ are affected in opposite ways by changes in
249 cytoskeletal tension.

250 The opposing effects of changes in myosin activity on myosin and β_H-Spec localization,
251 together with the observation that loss of β_H-Spec leads to increased myosin activity and apical
252 localization, raised the possibility that myosin and β_H-Spec compete for localization to apical F-
253 actin. To further investigate this possibility, we overexpressed β_H-Spec using a CRISPR-
254 activator (CRISPRa) approach. This involves the expression of a transcriptional activator fused
255 to dCas9 under UAS control, which can then be recruited to a gene of interest using a single-
256 guide RNA (sgRNA) targeted upstream of the transcription start site (Jia et al., 2019; Jia et al.,
257 2018). To verify the overexpression of β_H-Spec, we employed it in flies with GFP-tagged β_H-
258 Spec at the endogenous locus (Kst:GFP). To avoid excessive cell death caused by Kst
259 overexpression we expressed this construct under inducible conditions, using the temperature-
260 sensitive Gal4 repressor Gal80^{ts}. Both imaging and western blotting of wing discs confirmed that
261 this CRISPRa approach effectively increased expression of Kst:GFP (Figure 7 - figure
262 supplemental 1A-B). Examination of myosin under β_H-Spec overexpression conditions, using
263 Sqh:GFP, revealed a substantial reduction of myosin localization to AJs (Figure 7A, C, E-F), and
264 a reduction in tension along cell junctions as assayed by the recoil speed after laser cutting
265 (Figure 7I). Apical cell areas were also increased, consistent with a reduction of junctional
266 tension (Figure 7B and Fig 7-supplement1). As an independent method to overexpress β_H-Spec,
267 we used a previously described EP-element insertion near *kst*, P[EPgy2]EY01010 (UAS-kst^{EP})
268 (Pogodalla et al., 2021). Over-expression of β_H-Spec using UAS-kst^{EP} under *en-Gal4* control
269 also reduced myosin levels at AJ (Figure 7 – figure supplement 1C), although the effect appeared
270 weaker than that induced by the CRISPRa approach. These results provide further evidence that
271 β_H-Spec antagonizes myosin recruitment to AJs and establish that this effect can be observed
272 under both increased and decreased β_H-Spec expression conditions.

273 Consistent with these reductions in apical myosin accumulation, β_H-Spec overexpression
274 also reduced junctional recruitment of Jub (Figure 7B,D,G,H and Figure 7 – figure supplement
275 1D) and decreased wing size (wings were 92% and 89% of *nub-Gal4 UAS-dcr2* control size, for
276 the two different overexpression constructs) (Figure 3I-K).
277
278 **β_H-Spec and myosin compete for binding to F-actin**
279 The reciprocal antagonism between myosin and β_H-Spec suggested that they could
280 compete for binding to F-actin. β_H-Spec contains two N-terminal actin-binding domains, CH1
281 and CH2 (Liem, 2016), and myosin contains an actin-binding region in its motor domain (Duan
282 et al., 2018). While spectrins and myosin have been purified and characterized in vitro, we lack a
283 mechanistic understanding of the interaction between β_H-Spec and F-actin and how it might
284 affect myosin binding. To address this, we conducted in vitro co-sedimentation assays with
285 purified protein domains and F-actin. We found that the isolated *Drosophila* β_H-Spec actin-
286 binding region binds F-actin weakly (Figure 8A), in agreement with previous reports of F-actin
287 binding by other spectrin CH1-CH2 domains (Avery et al., 2017; Duan et al., 2018).
288 Constitutively active *Drosophila* Myosin II (subfragment-1-like protein) binding to F-actin
289 appears stronger than β_H-Spec binding, as at the same concentration a greater fraction of Myosin
290 II is bound to F-actin (Figure 8A,B). To investigate the antagonism between these proteins
291 observed in vivo, we performed biochemical competition assays between the β_H-Spec CH
292 domains and myosin for binding to F-actin. F-actin was preincubated with an excess of β_H-Spec
293 CH domains to maximize binding to F-actin, and then increasing concentrations of myosin were
294 added. We found that myosin can displace the actin-binding region of β_H-Spec from F-actin by
295 ~50% at the highest myosin concentration that we could use (Figure 8C, bottom right). Myosin

296 binding to F-actin was unaffected by preincubation with β_H-Spec CH domains (Figure 8 – figure
297 supplement 1A), likely due to active myosin's higher binding affinity for F-actin.

298 To gain a structural understanding of the antagonism between β_H-Spec and myosin we
299 built homology models of the *Drosophila* CH1-CH2 domain of β_H-Spec and the myosin II motor
300 domain and compared them with previous cryo-EM structures of the human actin-bound β-III-
301 spectrin actin binding CH1 domain and actin-bound myosin (Avery et al., 2017; von der Ecken
302 et al., 2016). The superimposition of the isolated *Drosophila* β_H-Spec CH1 domain model on the
303 human β-III spectrin CH1 domain in a complex with F-actin structure revealed a binding site
304 between actin subdomains (SD) SD1 and SD2 along the filament (Figure 8D). The binding
305 region of myosin on F-actin includes SD1, SD2, and SD3 (Figure 8D'). The superimposition of
306 both models suggests that the binding position of the CH1 domain on F-actin sterically interferes
307 with the formation of a strong actin-myosin interface (Figure 8D''). Modeling of the β_H-Spec
308 CH1-CH2 domain indicates that the CH2 domain presents additional steric hindrance for myosin
309 binding to F-actin (Figure 8 – figure supplement 1B-B''). Thus, structural modeling suggests that
310 the binding of spectrin or myosin to individual binding sites on F-actin is mutually exclusive,
311 which could explain why they compete for F-actin association in vivo and in vitro.

312

313 **DISCUSSION**

314 Multiple models for how spectrins regulate Hippo signaling have been proposed (Deng et
315 al., 2015; Deng et al., 2020; Fletcher et al., 2015; Wong et al., 2015). We focused on
316 investigating claims that spectrins could alter cytoskeletal tension in wing discs by regulating
317 pMLC levels without affecting localization of myosin or Jub (Deng et al., 2015). In contrast to
318 prior studies, we observed that when β_H-Spec or α-Spec levels are decreased by RNAi, levels of

319 junctional myosin are increased. This increase in junctional myosin levels is associated with
320 increased junctional tension and with increased recruitment of Jub to AJ. We are not certain why
321 these effects were missed in prior studies, but we note that our observations are consistent with
322 studies linking recruitment of both myosin and Jub to AJ under tension (Alegot et al., 2019;
323 Fernandez-Gonzalez et al., 2009; Ibar et al., 2018; Noll et al., 2017; Rauskolb et al., 2019;
324 Rauskolb et al., 2014; Razzell et al., 2018; Sarpal et al., 2019). Moreover, our results are further
325 supported by the observation that *jub* is genetically required for the influence of spectrin
326 knockdown on Yki activity and wing growth. Taken together, these observations imply that β_H-
327 Spec and α-Spec regulate Hippo signaling in wing discs through the Jub-biomechanical pathway,
328 rather than through hypothesized alternate mechanisms.

329 Spectrin has been suggested to form two distinct complexes in *Drosophila* epithelial
330 cells, $(\alpha\beta)_2$ and $(\alpha\beta_H)_2$ heterotetramers, which localize to the lateral and apical sides of cells,
331 respectively (Deng et al., 2015; Dubreuil et al., 1997; Fletcher et al., 2015; Lee et al., 1997;
332 Thomas et al., 1998; Zarnescu and Thomas, 1999). However, our observations indicate that β_H-
333 Spec functions independently of α-Spec in wing imaginal discs. α-Spec and β_H-Spec do not
334 exhibit significant co-localization. Moreover, α-Spec and β_H-Spec are not required for each
335 other's localization to apical cell junctions. This contrasts with the requirement for β-Spec for
336 recruitment of α-Spec to lateral membranes in wing discs. The requirement is not entirely
337 reciprocal, as α-Spec knockdown only partially reduces β-Spec recruitment, but this likely
338 reflects mechanisms that recruit spectrins to cell membranes: β-spectrin subunits, but not α-
339 spectrin subunits, have a pleckstrin homology domain that can mediate membrane association, as
340 well as possessing the CH domains that mediate F-actin association. Thus β-Spec can associate

341 with lateral membranes without α-Spec, but α-Spec does not have a way to associate with lateral
342 membranes without β-Spec.

343 An independent role for β_H-Spec has also been suggested in mammalian photoreceptors,
344 where it was reported that that mammalian βV-Spec does not colocalize with αII-Spectrin, and
345 that βV-Spec could form homodimers, potentially allowing it to cross-link actin by itself,
346 enabling α-Spec-independent functions (Papal et al., 2013). The observation that a mutation
347 in *Drosophila* α-Spec that disrupts binding to β-Spec *in vitro* has only mild phenotypes also
348 suggests that spectrin functions do not depend entirely on αβ interactions (Khanna et al., 2015).
349 Collectively, our results together with these earlier studies emphasize that the dogma that
350 "Spectrin comprises α-and β-subunits that interact in an antiparallel manner to form an αβ dimer"
351 (Liem, 2016) should be revised. Nonetheless, our results do not exclude the possibility that β_H-
352 Spec and α-Spec might act together in a physical complex in other tissues, or under distinct
353 physiological conditions.

354 The conclusion that β_H-Spec and α-Spec act independently in wing discs implies that they
355 influence tension at apical junctions through distinct mechanisms. We suggest that α-Spec could
356 influence AJ tension in wing discs through the mechanism proposed to explain the influence of
357 α- and β-Spec in pupal eyes (Deng et al., 2020). It was inferred that α- and β-Spec maintain cell
358 rigidity by linking F-actin to membranes. In the absence of α- or β-Spec, it was proposed that
359 dissociation between F-actin and the membrane leads to an expansion of the apical regions. This
360 expansion increases cytoskeletal tension at AJs, which bind F-actin independently of spectrins.
361 Consistent with this suggested mechanism, we observed a decrease in cell height in α-Spec
362 knockdown cells in wing discs, in conjunction with increased tension at apical junctions. The

363 alteration in cell shape was not observed in β_H-Spec knockdown cells, further supporting the
364 conclusion that β_H-Spec and α-Spec act in different ways to regulate junctional tension.

365 Instead, our experiments analyzing the relationship between β_H-Spec and myosin
366 revealed an entirely different mechanism by which β_H-Spec influences tension at AJ. We
367 observed a mutual antagonism between β_H-Spec and myosin *in vivo* for localization to apical F-
368 actin: decreasing β_H-Spec increases junctional myosin, while increasing β_H-Spec decreases
369 junctional myosin. Reciprocally, increasing myosin activity decreases β_H-Spec localization to
370 apical F-actin, while decreasing myosin activity increases β_H-Spec localization to apical F-
371 actin. In vitro studies with purified protein domains revealed that myosin can compete with β_H-
372 Spec for binding to F-actin. Finally, computational modeling of protein structures revealed that
373 myosin and β_H-Spec would interfere with each other's binding to F-actin. Together, these
374 observations indicate that β_H-Spec and myosin can directly compete with each other for
375 localization to F-actin. We suggest therefore that the influence of β_H-Spec on junctional tension
376 is likely to be a direct consequence of its competition with myosin for overlapping binding sites
377 on F-actin.

378 Despite β_H-Spec and myosin sharing overlapping binding sites on F-actin, and competing
379 reciprocally in vivo, in our co-sedimentation experiments we could only detect a partial ability of
380 myosin to compete for β_H-Spec binding, and we could not detect an ability of β_H-Spec to
381 compete for myosin binding. Several factors are likely to contribute to these observations. First,
382 we could not use higher protein concentrations of myosin or β_H-Spec due to the need to keep the
383 salt concentration constant and close to physiological levels, and to prevent protein precipitation.
384 Second, it has been suggested for β-Spec that the CH2 domain regulates the actin binding
385 function of the CH1 domain through steric hindrance when the two domains are associated

386 (Avery et al., 2017). A specific mutation in β-Spec CH2 (L253P) has been shown to lower the
387 energetic barrier between closed and open structural states, increasing the affinity of β-Spec for
388 F-actin around 1000-fold (Avery et al., 2016), but it is unknown how β-Spec or β_H-Spec
389 conformational changes are normally regulated in vivo and whether both proteins share this
390 regulatory feature. Additionally, phosphorylation of myosin regulatory light chain shifts myosin
391 from a compact, autoinhibited conformation to a filamentous, active conformation (Kiehart and
392 Feghali, 1986; Vasquez et al., 2016). The autoinhibited conformation binds F-actin very weakly
393 (K_D>100 μM) (Heissler and Manstein, 2013; Sellers et al., 1982) compared to the active
394 conformation, suggesting that spectrin could outcompete autoinhibited myosin more effectively
395 than active myosin for binding to F-actin. Our in vitro experiments used an active form of
396 myosin. In addition, other factors including other actin-binding proteins and cytoskeletal tension
397 are likely to influence the dynamic localization and actin-binding properties of both proteins
398 (Duan et al., 2018; Greenberg et al., 2016).

399 The competition between β_H-Spec and myosin also provides key insights into how β_H-
400 Spec contributes to ratcheting of apical constriction. The apical constriction of cells in the ventral
401 furrow that initiates *Drosophila* mesoderm invagination occurs through fast constriction pulses
402 interrupted by pauses during which cells must stabilize their constricted state before reinitiating
403 constriction (Martin et al., 2009; Xie and Martin, 2015). This ratcheting-like behavior is thought
404 to be a consequence of the finite length of actin filaments. Myosin contracts the cytoskeleton by
405 driving filaments past each other, and extensive contractions require release and reassociation
406 with new pairs of filaments. β_H-Spec participates in ratcheting of apical constriction (Krueger et
407 al., 2020). When β_H-Spec is knocked down, cells can undergo cycles of unratcheted apical
408 constriction during which they alternately constrict and then expand. Consequently, most β_H-

409 Spec depleted embryos fail to complete normal mesoderm invagination. It was proposed that the
410 actin cross-linking function of β_H-Spec could hold F-actin in place for the next cycle of myosin
411 mediated-contraction, but this raises the question of how myosin and β_H-Spec association with F-
412 actin are coordinated so that β_H-Spec prevents relaxation without interfering with constriction.
413 Our results suggest a simple solution: since they compete for the same binding site, the release of
414 myosin from F-actin at the end of a cycle of contraction would naturally be coupled to the
415 accessibility of F-actin for binding by β_H-Spec. Thus the competition between myosin and β_H-
416 Spec for binding to F-actin enables myosin-mediated cell contraction to effectively alternate with
417 β_H-Spec-mediated stabilization.
418

419 **MATERIALS AND METHODS**

420 ***Drosophila* genetics**

421 Unless otherwise indicated, crosses were performed at 29°C. Protein localization and
422 expression levels were monitored using previously characterized transgenes: *ex-lacZ*
423 (Hamaratoglu et al., 2006), *kst:YFP* (Lye et al., 2014), *kst:GFP* (Nagarkar-Jaiswal et al., 2015),
424 *jub:GFP* (Sabino et al., 2011), *sqh:GFP* (Royou et al., 2004), *sqh:mCherry* (Martin et al., 2009)
425 and *β-Spec:GFP* (II) (this paper).

426 To manipulate gene expression in the posterior compartment, *en-Gal4 UAS-RFP; UAS-*
427 *dcr2* flies were crossed with to UAS-RNAi or overexpression lines. RNAi transgenes used were
428 *UAS-kstRNAi* (v37075), *UAS-kstRNAi* (HMS00882), *UAS-α-specRNAi* (v25387), *UAS-β-*
429 *specRNAi* (GL01174), *UAS-rokRNAi* (v104675) and *UAS-jubRNAi* (v38442). To increase
430 myosin activity, we used *UAS-sqh*^{EE} (Winter et al., 2001), and to increase β_H-Spec levels, we
431 used *UAS-kstCRISPRa* (II) (this paper) and *UAS-kst*$^{P[EPgy2]EY01010}$ (Pogodalla et al., 2021).

432

433 **DNA Cloning**

434 To overexpress β_H-Spec *(UAS-kstCRISPRa)*, we used a second-generation
435 CRISPR/Cas9-transcriptional activation approach (Jia et al., 2018), allowing us to recruit the
436 transcriptional machinery near the transcription start site (TSS) of *kst* under UAS control. For
437 this, we made the following primers to generate a gRNA located less than 400 nt from the TSS:
438 5'-TTCGGATAAGCCGACAGGGTCTAT and 5'-AAACATAGACCCTGTCGGCTTATC-3'
439 These primers were duplexed and cloned in the FlySAM 2.0 vector using the BbsI site (Jia et al.,
440 2019). Transgenic flies were made by injection, inserting the construct into the attP40 site
441 (BestGene).

442 The actin binding domain (aa 1-278) of *kst* was cloned into pGEX-3X at the EcoRI site,
443 using the following primers: 5'-gatctgatcgaaggtcgtggaATGACCCAGCGGGACGGC-3' and 5'-
444 atcgtcagtcagtcacgatgTTACTTCTTGCGATCTGCGTCCATTAGC-3', and assembled using
445 NEBuilder® HiFi DNA Assembly (New England Biolabs, E2621) to generate plasmid pGEX-
446 3X-ABDkst.

447 Recombineering was used to generate the β-Spec:GFP construct. A left homology arm
448 (LHA, 1 kb before the stop codon of β-Spec) and a right homology arm (RHA, 1 kb after the
449 stop codon of β-Spec) were cloned in pL452-cEGFP (Venken et al., 2008) by Gibson assembly
450 into EcoRI (for LHA) and NotI (for RHA) sites, respectively, using the following primers:
451 LHA_b-spec_FWD 5' gacctgcagccaagctatcgATACATGGCTGCCAAGGC 3'; LHA_b-
452 spec_REV 5' gatcggaattgggctgcaggCTTTTTCTTTAAAGTAAAAAACGATCTGC 3'; RHA_b-
453 spec_FWD 5' caagtaactagttctagagcAGTAACAGCCGTAACGCAAC 3' and RHA_b-spec_FWD

454 5' tggagctccaccgcggtggcCGGCAATTGGTGTACTTTAAAG 3'. The regions of the primers in
455 lowercase indicate homology with the vector.
456 To activate the recombination machinery, SW106 E. coli containing the P[acman] clone
457 CH322-20K3 (chloramphenicol resistant) (Venken et al., 2009) were incubated at 42ºC for 17
458 min before making electrocompetent cells. A fragment containing LHA-loxP-NeoR/KanR-loxP-
459 EGFP-RHA was amplified and electroporated into the cells. Recombinant clones were selected
460 by chloramphenicol/kanamycin resistance and then floxed by inducible Cre expression by adding
461 0.1% L-arabinose. The final construct (LHA-loxP-EGFP-RHA) was confirmed by Sanger
462 sequencing and injected for insertion in flies into the attP40 site (BestGene).
463
464 **Histology and Imaging**
465 For most experiments wing discs were fixed in 4% paraformaldehyde for 15 min at room
466 temperature. Sqh:GFP discs were fixed for 12 min. Primary antibodies used were mouse anti-α-
467 Spectrin (1:50, Developmental Studies Hybridoma Bank (DSHB), 3A9, deposited to the DSHB
468 by Branton, D. / Dubreuil, R., RRID:AB_528473), rabbit anti-β-spectrin (1:100, a gift from
469 Christian Klämbt) (Hulsmeier et al., 2007), rabbit anti-Dcr2 (1:800, Abcam, ab4732,
470 RRID:AB_449344), rabbit anti-pMLC (T18/S19) (1:50, Cell Signaling Technologies, #3671,
471 RRID:AB_330248), rat anti-E-cad (1:200, DSHB, DCAD2-c, deposited to the DSHB by
472 Uemura, T., RRID:AB_528120), mouse β-galactosidase (1:200, DSHB, JIE7, deposited to the
473 DSHB by Mason, T.L. / Partaledis, J.A., RRID:AB_528101). Secondary antibodies were used at
474 a 1:100 dilution, and included anti-rat Alexa Fluor 647 (Jackson ImmunoResearch, 712-605-153,
475 RRID:AB_2340694), anti-rabbit Alexa Flour 647 (Jackson ImmunoResearch, 711-605-152,
476 RRID:AB_2492288), anti-mouse Alexa Fluor 647 (Jackson ImmunoResearch, 715-605-151,

477 RRID:AB_2340863), anti-mouse Cy3 (Jackson ImmunoResearch, 715-165-151,
478 RRID:AB_2315777), anti-rabbit Cy3 (Jackson ImmunoResearch, 711-165-152,
479 RRID:AB_2307443), anti-rat Cy3 (Jackson ImmunoResearch, 712-165-153,
480 RRID:AB_2340667), anti-mouse Alexa Fluor 488 (Thermo Fisher Scientific, A-21202,
481 RRID:AB_141607) and anti-rabbit Alexa Flour 488 (Thermo Fisher Scientific, A-21206,
482 RRID:AB_2535792). DNA was stained using Hoechst (Invitrogen, H3570). Wing discs were
483 removed and mounted on a slide in Vectashield (Vector Laboratories, H-1000). Confocal images
484 were captured on a Leica SP8 microscope.
485
486 **Proximity Ligation Assay (PLA)**
487 PLA was performed with the Duolink® Proximity Ligation Assay kit according to the
488 manufacturer's instructions (Sigma). Fixation was performed as in the normal immunostaining
489 procedure. For the permeabilization step, 0.5% Triton X-100 in PBS was used in two washes of
490 20 min each. Antibodies used for PLA include rabbit anti-GFP (1:200; ChromoTek # PABG1-
491 20, RRID:AB_2749857)) and mouse α-Spectrin (1:50, Developmental Studies Hybridoma Bank,
492 3A9, RRID:AB_528473) antibodies, and secondary anti-mouse MINUS (Sigma-Aldrich Cat#
493 DUO92004, RRID:AB_2713942) and anti-rabbit PLUS (Sigma-Aldrich Cat# DUO92002,
494 RRID:AB_2810940) probes were used.
495
496 **Immunoblotting**
497 Wing discs (20 discs per lane) were lysed in 2× Laemmli Sample Buffer (Bio-Rad,
498 #1610737) supplemented with protease inhibitor cocktail (Roche) and phosphatase inhibitor
499 cocktail (Calbiochem). Protein samples were loaded in 4% to 15% gradient gels (Bio-Rad).

500 Antibodies used for immunoblotting include mouse anti-GFP (1:1000; Cell Signaling
501 Technology, #2955, RRID:AB_1196614) and as a loading control rabbit anti-GAPDH (1:5000;
502 Santa Cruz Biotechnology, sc-25778, RRID:AB_10167668). Blots were visualized with
503 fluorescent-conjugated secondary antibodies (LI-COR Biosciences) and the Odyssey Imaging
504 System (LICOR Biosciences).
505
506 **Laser ablation**

507 Live imaging and laser ablation experiments were performed as previously described
508 (Rauskolb et al., 2014). *en-Gal4 UAS-RFP/CyO; UAS-dcr2/TM6B* flies were crossed with *UAS-*
509 *kstRNAi; Ubi-E-cad:GFP/TM6B, UAS-a-specRNAi; Ubi-E-cad:GFP/TM6B* or *UAS-*
510 *kstCRISPRa; Ubi-E-cad:GFP/TM6B* flies. Eggs were collected at 25ºC for 4 hours and then
511 shifted to 29°C for 88 h. Wing disc culture was based on the procedure of (Dye et al., 2017). A
512 stock medium was prepared using Grace's medium (Sigma, G9771) without sodium bicarbonate
513 but with the addition of 5 mM Bis-Tris and the pH was adjusted to 6.6-6.7 at room temperature.
514 This was stored at 4°C for less than a month. Before every experiment, we added 5% fetal bovine
515 serum (FBS; ThermoFisher, 10082147), Penicillin-Streptomycin (Thermo-Fisher, #15070063,
516 100X stock solution) and 10 nM 20-hydroxy-ecdysone (Sigma, H5142) to the medium. Larvae
517 were floated on 25% sucrose and transferred into glass dishes with culture medium. Larvae of
518 the desired genotype were selected and sterilized in 70% ethanol for 1 min. Then, we drew a
519 circle on the glass bottom of a 35-mm glass-bottomed Petri dish (MatTek, P35G-0-14-C) using
520 glue made by mixing heptane with tape (Tesa, 5388). Wing discs were dissected out of larvae,
521 transferred into this Petri dish, and oriented using tungsten needles. Then we covered the discs
522 with a Cyclopore Polycarbonate membrane (GE Health, 7060-2513) and glued it to the glass

523 bottom to immobilize discs. Discs were imaged every 0.2 s on a Perkin Elmer Ultraview
524 spinning disc confocal microscope, and ablation of junctions was achieved using a Micropoint
525 pulsed laser (Andor Technology) tuned to 365 nm. Paired cutting of junctions, one in the anterior
526 compartment and another in the posterior compartment at a similar location, were performed and
527 compared. The displacement of vertices for the first second after ablation was used to calculate
528 the velocities.

529 **Quantification and Statistical Analysis**

530 To obtain the surface of the wing disc and remove signals from the peripodial epithelium,
531 we used the MATLAB toolbox ImSAnE (Heemskerk and Streichan, 2015) to detect and isolate a
532 slice of the disc epithelium that surrounds the adherens junctions, using E-cad as a reference, as
533 described previously (Pan et al., 2016). The KstGFP, KstYFP, SqhGFP and JubGFP images were
534 created using ImSAnE.

535 For the fluorescence intensity heat maps, a custom MATLAB script was used (Alegot et
536 al., 2019; Pan et al., 2018) (https://github.com/alegoth/Wing-disc-Intensity-Analysis). The script
537 generates a 3D mask with the normalization channel (E-cad) keeping only the relevant pixels.
538 The wing disc center (intersection between AP/DV boundaries) is picked for each image
539 manually. Then, the picture is split into blocks of a given *xy* size (3×3 μm), starting from the
540 center, and the average intensity per pixel of each channel is measured. The intensity of the
541 reference channel and the channel of interest are normalized over their respective average
542 intensity. The ratio of the channel of interest over the reference channel is then determined. To
543 average several discs, only matrices of the same *xy* size blocks were used. The center of the disc
544 serves as a reference point; smaller matrices were expanded to correspond to the size of the
545 biggest matrix and filled with NaN (Not-a-Number). We determined the minimum number of

546 values required (usually three) to average the ratio for a given position. This means that the
547 edges of the average disk are composed of the same minimum number of values, which
548 corresponds to the *n* given for each experiment. Finally, signals from several wing discs were
549 averaged and represented by the heat map, and a posterior versus anterior ratio was calculated.

550 Pearson's correlation coefficient was calculated to establish co-localization between
551 different proteins by using the Coloc 2 Plugin for ImageJ (https://imagej.net/plugins/coloc-2).

552 Statistical significance was determined with GraphPad Prism software by performing
553 Student's t-test (for comparison between two observations) or analysis of variance (ANOVA)
554 with $P<0.05$ set as the criteria for significance. The Dunnett test was used to derive adjusted P-
555 values for comparisons against the control experimental value, and the Tukey test was used to
556 derive adjusted P-values for multiple comparisons.

557

558 **Protein production and purification**

559 To purify the actin binding domain of β_H-Spec fused with GST, we transformed BL21-
560 DE3 cells (NEB) with pGEX-3X-ABDkst. Protein expression was induced with 0.2 mM
561 isopropyl-β-D-thiogalactoside (IPTG) at room temperature for 12–15 h. Cells were harvested and
562 lysed by sonication in lysis buffer: PBS (pH 7.4), 1% Triton X-100, 5 mM dithiothreitol, 1 mM
563 phenylmethyl sulfonyl fluoride and complete Mini Protease Inhibitor Cocktail (Roche). After
564 centrifugation, the supernatant was collected and passed through a 1 mL GST-Trap column
565 (Cytiva) at 4 °C. Then, the column was washed with PBS (pH 7.4) until the absorbance reached a
566 steady baseline. To remove the GST-tag, the column was loaded with 80 units of Factor Xa
567 (New England Biolabs, P8010) in cleavage buffer: 50 mM Tris-HCl, 150 mM NaCl, 1 mM
568 $CaCl_2$, pH 7.5 and incubated for 16 h at room temperature. To elute the ABD of β_H-Spec while

569 removing the protease simultaneously, we used a HiTrap Benzamidine FF (Cytiva) column in
570 tandem with the GST-trap column and eluted the ABD of β_H-spec with cleavage buffer. To
571 switch buffers, we dialyzed the protein against 25 mM HEPES pH 7.4, 150 mM NaCl, 1 mM
572 TCP overnight. Then the purified protein was concentrated by ultrafiltration to 30 µM and stored
573 at -80ºC until used in experiments.

574 G-actin was prepared from rabbit muscle acetone powder as reported (Lehrer and
575 Kerwar, 1972) and further purified with size exclusion chromatography on a Superdex 75 pg
576 column (Cytiva, # 28989333) in buffer containing 5 mM Tris/HCl pH=8, 0.2 mM $CaCl_2$, 0.5
577 mM ATP, 1 mM DTT. G-actin was polymerized to F-actin by the addition of 10X
578 polymerization buffer (100 mM HEPES pH 7.0, 500 mM KCl, 20 mM $MgCl_2$, 10 mM EDTA).
579 *Drosophila* nonmuscle myosin-2 subfragment-1-like protein (*Zip*, amino acids 1-813) was
580 recombinantly overproduced together with the myosin regulatory (*Sqh*) and essential light chain
581 (*Mlc-c*) in the baculovirus/*Sf*9 insect cell system (Thermo Fisher Scientific) and prepared as
582 described (Heissler et al., 2015).

583

584 **Co-sedimentation assays**

585 For co-sedimentation assays, β_H-Spec CH domains or myosin were incubated with F-
586 actin for 15 mins at room temperature in an assay buffer containing 10 mM HEPES pH 7.4, 100
587 mM NaCl, 0.1 mM EGTA, 20µM ATP and 1 mM DTT and subsequently sedimented (100,000 x
588 g, 15 min, 4°C, TLA-100 rotor) in an Ultima MAX-XP ultracentrifuge (Beckman). For
589 competition assays, β_H-Spec and actin were preincubated for 15 mins at room temperature before
590 the addition of myosin. Supernatant and pellet fractions were separated and the pellet fraction
591 was resuspended in an equal volume of assay buffer. Samples were supplemented with NuPAGE

592 LDS sample buffer (Invitrogen, #NP0007) and heated for 10 min at 90°C. Supernatant and pellet
593 fractions were resolved on 4-12% NuPAGE Bis-Tris polyacrylamide gels (Invitrogen,
594 NP0323BOX). Gels were incubated with PageBlue protein staining solution (Thermo Scientific,
595 #24620) and destained with water. Gels were documented with a ChemiDoc MP (Bio-Rad) and
596 densitometric analysis was performed with Fiji (Schindelin et al., 2012). Data plots and
597 secondary analysis were performed in Origin 2019.
598

599 **Model building**

600 A homology model of the *Drosophila* myosin motor domain (*Zip*, amino acids 1-813) in
601 the actin-bound state was modeled using the cryo-EM structure of the human nonmuscle myosin-
602 2C motor domain in the rigor state (PDB entry: 5JLH) as a template. Both motor domains share
603 ~ 72% sequence identity at the amino acid level. The motor domain model was built using
604 Modeler (Sali and Blundell, 1993). The model of the *Drosophila* β_H-Spectrin calponin homology
605 domain tandem (CH1-CH2, amino acids 1-278) was modeled using ColabFold (Mirdita et al.,
606 2022). This model was superimposed onto the cryo-EM structure of the human β-III spectrin
607 CH1 domain bound to F-actin (PDB entry: 6ANU) for binding site analysis.
608

609 **ACKNOWLEDGEMENTS**

610 We thank Christian Klämbt for the β-Spec antibody, and Richard Ebright and Bryce Nickels for
611 sharing equipment for protein purification. This research was supported by National Institutes of
612 Health grants GM131748 (KDI) and R01GM143539 (KC).
613

614 **DATA and MATERIAL AVAILABILITY**

615 All data generated or analyzed during this study are included in the manuscript and supporting
616 files. All material including plasmids and transgenic fly lines generated in this study are
617 available on request or through public repositories.

618

619 **REFERENCES**

620

621 **Alegot, H., Markosian, C., Rauskolb, C., Yang, J., Kirichenko, E., Wang, Y. C. and Irvine,**
622 **K. D.** (2019). Recruitment of Jub by alpha-catenin promotes Yki activity and Drosophila
623 wing growth. *J Cell Sci* **132**.

624 **Aragona, M., Panciera, T., Manfrin, A., Giulitti, S., Michielin, F., Elvassore, N., Dupont, S.**
625 **and Piccolo, S.** (2013). A mechanical checkpoint controls multicellular growth through
626 YAP/TAZ regulation by actin-processing factors. *Cell* **154**, 1047-1059.

627 **Avery, A. W., Crain, J., Thomas, D. D. and Hays, T. S.** (2016). A human beta-III-spectrin
628 spinocerebellar ataxia type 5 mutation causes high-affinity F-actin binding. *Sci Rep* **6**,
629 21375.

630 **Avery, A. W., Fealey, M. E., Wang, F., Orlova, A., Thompson, A. R., Thomas, D. D., Hays,**
631 **T. S. and Egelman, E. H.** (2017). Structural basis for high-affinity actin binding
632 revealed by a beta-III-spectrin SCA5 missense mutation. *Nat Commun* **8**, 1350.

633 **Das Thakur, M., Feng, Y., Jagannathan, R., Seppa, M. J., Skeath, J. B. and Longmore, G.**
634 **D.** (2010). Ajuba LIM proteins are negative regulators of the Hippo signaling pathway.
635 *Curr Biol* **20**, 657-662.

636 **Deng, H., Wang, W., Yu, J., Zheng, Y., Qing, Y. and Pan, D.** (2015). Spectrin regulates Hippo
637 signaling by modulating cortical actomyosin activity. *Elife* **4**, e06567.

638 **Deng, H., Yang, L., Wen, P., Lei, H., Blount, P. and Pan, D.** (2020). Spectrin couples cell
639 shape, cortical tension, and Hippo signaling in retinal epithelial morphogenesis. *J Cell*
640 *Biol* **219**.

641 **Dietzl, G., Chen, D., Schnorrer, F., Su, K. C., Barinova, Y., Fellner, M., Gasser, B., Kinsey,**
642 **K., Oppel, S., Scheiblauer, S., et al.** (2007). A genome-wide transgenic RNAi library
643 for conditional gene inactivation in Drosophila. *Nature* **448**, 151-156.

644 **Duan, R., Kim, J. H., Shilagardi, K., Schiffhauer, E. S., Lee, D. M., Son, S., Li, S., Thomas,**
645 **C., Luo, T., Fletcher, D. A., et al.** (2018). Spectrin is a mechanoresponsive protein
646 shaping fusogenic synapse architecture during myoblast fusion. *Nat Cell Biol* **20**, 688-
647 698.

648 **Dubreuil, R., Byers, T. J., Branton, D., Goldstein, L. S. and Kiehart, D. P.** (1987).
649 Drosophilia spectrin. I. Characterization of the purified protein. *J Cell Biol* **105**, 2095-
650 2102.

651 **Dubreuil, R. R., Maddux, P. B., Grushko, T. A. and MacVicar, G. R.** (1997). Segregation of
652 two spectrin isoforms: polarized membrane-binding sites direct polarized membrane
653 skeleton assembly. *Mol Biol Cell* **8**, 1933-1942.

654 **Dye, N. A., Popovic, M., Spannl, S., Etournay, R., Kainmuller, D., Ghosh, S., Myers, E. W.,**
655 **Julicher, F. and Eaton, S.** (2017). Cell dynamics underlying oriented growth of the
656 Drosophila wing imaginal disc. *Development* **144**, 4406-4421.

657 **Fernandez, B. G., Gaspar, P., Bras-Pereira, C., Jezowska, B., Rebelo, S. R. and Janody, F.**
658 (2011). Actin-Capping Protein and the Hippo pathway regulate F-actin and tissue growth
659 in Drosophila. *Development* **138**, 2337-2346.

660 **Fernandez-Gonzalez, R., Simoes, S. d. M., Röper, J.-C., Eaton, S. and Zallen, J. A.** (2009).
661 Myosin II dynamics are regulated by tension in intercalating cells. *Developmental Cell*
662 **17**, 736-743.

663 **Fletcher, G. C., Elbediwy, A., Khanal, I., Ribeiro, P. S., Tapon, N. and Thompson, B. J.**
664 (2015). The Spectrin cytoskeleton regulates the Hippo signalling pathway. *EMBO J* **34**,
665 940-954.

666 **Forest, E., Logeay, R., Geminard, C., Kantar, D., Frayssinoux, F., Heron-Milhavet, L. and**
667 **Djiane, A.** (2018). The apical scaffold big bang binds to spectrins and regulates the
668 growth of Drosophila melanogaster wing discs. *J Cell Biol* **217**, 1047-1062.

669 **Greenberg, M. J., Arpag, G., Tuzel, E. and Ostap, E. M.** (2016). A Perspective on the Role of
670 Myosins as Mechanosensors. *Biophys J* **110**, 2568-2576.

671 **Hamaratoglu, F., Willecke, M., Kango-Singh, M., Nolo, R., Hyun, E., Tao, C., Jafar-Nejad,**
672 **H. and Halder, G.** (2006). The tumour-suppressor genes NF2/Merlin and Expanded act
673 through Hippo signalling to regulate cell proliferation and apoptosis. *Nat Cell Biol* **8**, 27-
674 36.

675 **Heemskerk, I. and Streichan, S. J.** (2015). Tissue cartography: compressing bio-image data by
676 dimensional reduction. *Nat Methods* **12**, 1139-1142.

677 **Heissler, S. M., Chinthalapudi, K. and Sellers, J. R.** (2015). Kinetic characterization of the
678 sole nonmuscle myosin-2 from the model organism Drosophila melanogaster. *FASEB J*
679 **29**, 1456-1466.

680 **Heissler, S. M. and Manstein, D. J.** (2013). Nonmuscle myosin-2: mix and match. *Cell Mol*
681 *Life Sci* **70**, 1-21.

682 **Hulsmeier, J., Pielage, J., Rickert, C., Technau, G. M., Klambt, C. and Stork, T.** (2007).
683 Distinct functions of alpha-Spectrin and beta-Spectrin during axonal pathfinding.
684 *Development* **134**, 713-722.

685 **Ibar, C., Kirichenko, E., Keepers, B., Enners, E., Fleisch, K. and Irvine, K. D.** (2018).
686 Tension-dependent regulation of mammalian Hippo signaling through LIMD1. *J Cell*
687 *Science* **131**, jcs214700.

688 **Jia, Y., Shen, D., Wang, X., Sun, J., Peng, P., Xu, R. G., Xu, B. and Ni, J. Q.** (2019). flySAM
689 Transgenic CRISPRa System Manual. *Bio Protoc* **9**, e3147.

690 **Jia, Y., Xu, R. G., Ren, X., Ewen-Campen, B., Rajakumar, R., Zirin, J., Yang-Zhou, D.,**
691 **Zhu, R., Wang, F., Mao, D., et al.** (2018). Next-generation CRISPR/Cas9
692 transcriptional activation in Drosophila using flySAM. *Proc Natl Acad Sci U S A* **115**,
693 4719-4724.

694 **Khanna, M. R., Mattie, F. J., Browder, K. C., Radyk, M. D., Crilly, S. E., Bakerink, K. J.,**
695 **Harper, S. L., Speicher, D. W. and Thomas, G. H.** (2015). Spectrin tetramer formation
696 is not required for viable development in Drosophila. *J Biol Chem* **290**, 706-715.

697 **Kiehart, D. P. and Feghali, R.** (1986). Cytoplasmic myosin from Drosophila melanogaster. *J*
698 *Cell Biol* **103**, 1517-1525.

699 **Krueger, D., Pallares Cartes, C., Makaske, T. and De Renzis, S.** (2020). betaH-spectrin is
700 required for ratcheting apical pulsatile constrictions during tissue invagination. *EMBO*
701 *Rep* **21**, e49858.

702 **Lee, J. K., Brandin, E., Branton, D. and Goldstein, L. S.** (1997). alpha-Spectrin is required for
703 ovarian follicle monolayer integrity in Drosophila melanogaster. *Development* **124**, 353-
704 362.

705 **Lehrer, S. S. and Kerwar, G.** (1972). Intrinsic fluorescence of actin. *Biochemistry* **11**, 1211-
706 1217.

707 **Liem, R. K.** (2016). Cytoskeletal Integrators: The Spectrin Superfamily. *Cold Spring Harb*
708 *Perspect Biol* **8**.

709 **Lye, C. M., Naylor, H. W. and Sanson, B.** (2014). Subcellular localisations of the CPTI
710 collection of YFP-tagged proteins in Drosophila embryos. *Development* **141**, 4006-4017.

711 **Machnicka, B., Czogalla, A., Hryniewicz-Jankowska, A., Boguslawska, D. M.,**
712 **Grochowalska, R., Heger, E. and Sikorski, A. F.** (2014). Spectrins: a structural
713 platform for stabilization and activation of membrane channels, receptors and
714 transporters. *Biochim Biophys Acta* **1838**, 620-634.

715 **Martin, A. C., Kaschube, M. and Wieschaus, E. F.** (2009). Pulsed contractions of an actin-
716 myosin network drive apical constriction. *Nature* **457**, 495-499.

717 **Mirdita, M., Schutze, K., Moriwaki, Y., Heo, L., Ovchinnikov, S. and Steinegger, M.** (2022).
718 ColabFold: making protein folding accessible to all. *Nat Methods* **19**, 679-682.

719 **Misra, J. R. and Irvine, K. D.** (2018). The Hippo Signaling Network and its Biological
720 Functions. *Annual Reviews of Genetics* **52**, 3.1-3.23.

721 **Nagarkar-Jaiswal, S., Lee, P. T., Campbell, M. E., Chen, K., Anguiano-Zarate, S.,**
722 **Gutierrez, M. C., Busby, T., Lin, W. W., He, Y., Schulze, K. L., et al.** (2015). A
723 library of MiMICs allows tagging of genes and reversible, spatial and temporal
724 knockdown of proteins in Drosophila. *Elife* **4**.

725 **Noll, N., Mani, M., Heemskerk, I., Streichan, S. J. and Shraiman, B. I.** (2017). Active
726 tension network model suggests an exotic mechanical state realized in epithelial tissues.
727 *Nature Physics* **13**, 1221-1226.

728 **Pan, Y., Alegot, H., Rauskolb, C. and Irvine, K. D.** (2018). The dynamics of Hippo signaling
729 during Drosophila wing development. *Development* **145**.

730 **Pan, Y., Heemskerk, I., Ibar, C., Shraiman, B. I. and Irvine, K. D.** (2016). Differential
731 growth triggers mechanical feedback that elevates Hippo signaling. *Proc Natl Acad Sci U*
732 *S A* **113**, E6974-E6983.

733 **Papal, S., Cortese, M., Legendre, K., Sorusch, N., Dragavon, J., Sahly, I., Shorte, S.,**
734 **Wolfrum, U., Petit, C. and El-Amraoui, A.** (2013). The giant spectrin betaV couples
735 the molecular motors to phototransduction and Usher syndrome type I proteins along
736 their trafficking route. *Hum Mol Genet* **22**, 3773-3788.

737 **Pogodalla, N., Kranenburg, H., Rey, S., Rodrigues, S., Cardona, A. and Klambt, C.** (2021).
738 Drosophila ssHeavy-Spectrin is required in polarized ensheathing glia that form a
739 diffusion-barrier around the neuropil. *Nat Commun* **12**, 6357.

740 **Rauskolb, C., Cervantes, E., Madere, F. and Irvine, K. D.** (2019). Organization and function
741 of tension-dependent complexes at adherens junctions. *J Cell Sci* **132**.

742 **Rauskolb, C., Han, A., Kirichenko, E., Ibar, C. and Irvine, K. D.** (2022). Analysis of the
743 Drosophila Ajuba LIM protein defines functions for distinct LIM domains. *PLoS One* **17**,
744 e0269208.

745 **Rauskolb, C., Pan, G., Reddy, B. V., Oh, H. and Irvine, K. D.** (2011). Zyxin links fat
746 signaling to the hippo pathway. *PLoS Biol* **9**, e1000624.

747 **Rauskolb, C., Sun, S., Sun, G., Pan, Y. and Irvine, K. D.** (2014). Cytoskeletal tension inhibits
748 Hippo signaling through an Ajuba-Warts complex. *Cell* **158**, 143-156.

749 **Razzell, W., Bustillo, M. E. and Zallen, J. A.** (2018). The force-sensitive protein Ajuba
750 regulates cell adhesion during epithelial morphogenesis. *J Cell Biol*, jcb.201801171.

751 **Royou, A., Field, C., Sisson, J. C., Sullivan, W. and Karess, R.** (2004). Reassessing the role
752 and dynamics of nonmuscle myosin II during furrow formation in early Drosophila
753 embryos. *Mol Biol Cell* **15**, 838-850.

754 **Sabino, D., Brown, N. H. and Basto, R.** (2011). Drosophila Ajuba is not an Aurora-A activator
755 but is required to maintain Aurora-A at the centrosome. *J Cell Sci* **124**, 1156-1166.

756 **Sali, A. and Blundell, T. L.** (1993). Comparative protein modelling by satisfaction of spatial
757 restraints. *J Mol Biol* **234**, 779-815.

758 **Sansores-Garcia, L., Bossuyt, W., Wada, K., Yonemura, S., Tao, C., Sasaki, H. and Halder,**
759 **G.** (2011). Modulating F-actin organization induces organ growth by affecting the Hippo
760 pathway. *EMBO J* **30**, 2325-2335.

761 **Sarpal, R., Yan, V., Kazakova, L., Sheppard, L., Yu, J. C., Fernandez-Gonzalez, R. and**
762 **Tepass, U.** (2019). Role of α-Catenin and its mechanosensing properties in regulating
763 Hippo/YAP-dependent tissue growth. *PLoS Genet* **15**, e1008454.

764 **Schindelin, J., Arganda-Carreras, I., Frise, E., Kaynig, V., Longair, M., Pietzsch, T.,**
765 **Preibisch, S., Rueden, C., Saalfeld, S., Schmid, B., et al.** (2012). Fiji: an open-source
766 platform for biological-image analysis. *Nat Methods* **9**, 676-682.

767 **Sellers, J. R., Eisenberg, E. and Adelstein, R. S.** (1982). The binding of smooth muscle heavy
768 meromyosin to actin in the presence of ATP. Effect of phosphorylation. *J Biol Chem* **257**,
769 13880-13883.

770 **Sun, S., Reddy, B. V. and Irvine, K. D.** (2015). Localization of Hippo signalling complexes
771 and Warts activation in vivo. *Nat Commun* **6**, 8402.

772 **Thomas, G. H. and Kiehart, D. P.** (1994). Beta heavy-spectrin has a restricted tissue and
773 subcellular distribution during Drosophila embryogenesis. *Development* **120**, 2039-2050.

774 **Thomas, G. H., Zarnescu, D. C., Juedes, A. E., Bales, M. A., Londergan, A., Korte, C. C.**
775 **and Kiehart, D. P.** (1998). Drosophila betaHeavy-spectrin is essential for development
776 and contributes to specific cell fates in the eye. *Development* **125**, 2125-2134.

777 **Vasquez, C. G., Heissler, S. M., Billington, N., Sellers, J. R. and Martin, A. C.** (2016).
778 Drosophila non-muscle myosin II motor activity determines the rate of tissue folding.
779 *Elife* **5**.

780 **Venken, K. J., Carlson, J. W., Schulze, K. L., Pan, H., He, Y., Spokony, R., Wan, K. H.,**
781 **Koriabine, M., de Jong, P. J., White, K. P., et al.** (2009). Versatile P[acman] BAC
782 libraries for transgenesis studies in Drosophila melanogaster. *Nat Methods* **6**, 431-434.

783 **Venken, K. J., Kasprowicz, J., Kuenen, S., Yan, J., Hassan, B. A. and Verstreken, P.** (2008).
784 Recombineering-mediated tagging of Drosophila genomic constructs for in vivo
785 localization and acute protein inactivation. *Nucleic Acids Res* **36**, e114.

786 **von der Ecken, J., Heissler, S. M., Pathan-Chhatbar, S., Manstein, D. J. and Raunser, S.**
787 (2016). Cryo-EM structure of a human cytoplasmic actomyosin complex at near-atomic
788 resolution. *Nature* **534**, 724-728.

789 **Winter, C. G., Wang, B., Ballew, A., Royou, A., Karess, R., Axelrod, J. D. and Luo, L.**
790 (2001). Drosophila Rho-associated kinase (Drok) links Frizzled-mediated planar cell
791 polarity signaling to the actin cytoskeleton. *Cell* **105**, 81-91.

792 **Wong, K. K., Li, W., An, Y., Duan, Y., Li, Z., Kang, Y. and Yan, Y.** (2015). beta-Spectrin
793 regulates the hippo signaling pathway and modulates the basal actin network. *J Biol*
794 *Chem* **290**, 6397-6407.

795 **Xie, S. and Martin, A. C.** (2015). Intracellular signalling and intercellular coupling coordinate
796 heterogeneous contractile events to facilitate tissue folding. *Nat Commun* **6**, 7161.

797 **Zarnescu, D. C. and Thomas, G. H.** (1999). Apical spectrin is essential for epithelial
798 morphogenesis but not apicobasal polarity in Drosophila. *J Cell Biol* **146**, 1075-1086.

799 **Zheng, Y. and Pan, D.** (2019). The Hippo Signaling Pathway in Development and Disease. *Dev*
800 *Cell* **50**, 264-282.
801
802

803 **Figure Legends**

804

805 **Figure 1. Knockdown of β_H-Spec or α-Spec increases junctional myosin levels in wing discs**
806 (A-C) Apical sections of wing discs stained for E-cad (red/gray) expressing en-Gal4 UAS-RFP
807 UAS-dcr2 sqh:GFP crossed to control (Oregon-R, OR) (A), UAS-kstRNAi(v37075) (B), or
808 UAS-α-specRNAi (C) showing the effect on Sqh:GFP (green/gray) levels and localization in the
809 posterior compartment (marked by RFP, blue). Dashed yellow line marks A/P compartment
810 boundary. Scale bar = 20 μm; all images are at the same magnification. Panels to the right, in
811 gray, show single channels, as indicated. (D-F) Heat maps of relative junctional Sqh:GFP
812 intensity of wing discs. Average levels of Sqh:GFP relative to E-cad levels are shown for the
813 different genotypes analyzed in A-C. Heat map scale is indicated on the top. Number of wing
814 discs used for analysis: Control (OR), n=6; UAS-kstRNAi, n=5; UAS-α-specRNAi, n=6. (G)
815 Average recoil velocities after laser cutting of cell junctions in anterior (A) or posterior (P)
816 compartments of wing discs expressing UAS-kstRNAi or UAS-α-specRNAi in posterior cells
817 under en-Gal4 control (n=20). (H-I) Quantification of Sqh:GFP normalized to E-cadherin in
818 posterior cells (P) compared to anterior cells (A) in wing disc expressing the indicated
819 constructs, displayed as individual values, normalized by E-cad (H) or normalized by the mean
820 intensity of Sqh:GFP (I). Data are shown as mean ± 95% CI. Statistical significance in (G) was
821 determined by Student's t-test between A and P. For (H) and (I), statistical significance was
822 determined by a one-way ANOVA with Dunnett's multiple comparison test relative to the
823 control (Oregon-R): ns: not significant, *P<0.05; **P≤0.01; ***P≤0.001; ****P≤0.0001.

824

825

826 **Figure 1 – figure supplement 1. Validation of RNAi lines**
827 (A-B) horizontal (upper panels) and vertical (lower panels) sections of third instar wing imaginal
828 discs expressing en-Gal4 UAS-dcr2 Kst:YFP (green/gray) crossed with UAS-kstRNAi(v37075)
829 (A) and UAS-kstRNAi(HMS00882) (B), stained for E-cad (magenta). (C-D) Horizontal (upper
830 panels) and vertical (lower panels) sections of third instar wing imaginal discs expressing en-
831 Gal4 UAS-RFP (magenta) UAS-dcr2 crossed with UAS-α-specRNAi (C) or UAS-β-specRNAi
832 (D) immunostained with α-Spec antibody or β-Spec antibody, respectively (green/gray). Gray
833 scale images show the spectrin alone. β-specRNAi severely reduced β-Spec staining in most of

834 the wing disc but some signal remains near the peripodial membrane, which likely reflects non-
835 specific staining by the anti-sera. Scale bar = 20 µm.
836
837
838 **Figure 1 – figure supplement 2. Modulation of levels of total and active myosin in wing**
839 **discs by spectrins.**
840 (A-C) Apical sections of third instar wing imaginal discs expressing en-Gal4 UAS-dcr2 UAS-
841 RFP (blue) crossed with control (A), UAS-kstRNAi(v37075) (B) and UAS-α-SpecRNAi (C),
842 stained with pMLC antibody (green/gray) and E-cad (red/gray). (D) Quantification of pMLC
843 normalized to E-cadherin in posterior cells (P) compared to anterior cells (A) in wing discs
844 expressing the indicated constructs, displayed as individual values. Number of wing discs used
845 for analysis: Control (OR), n=5; UAS-kstRNAi, n=8, UAS-α-SpecRNAi, n=5. Error bars show
846 mean with 95% CI. Statistical significance was determined by one-way ANOVA with Dunnett's
847 multiple comparison test. Statistical comparisons are shown relative to the control (OR).
848 ***P≤0.001, ****P<0.0001. (E) Third instar wing imaginal discs expressing en-Gal4 UAS-dcr2
849 UAS-RFP (blue) sqh:GFP (green) in combination with UAS-kstRNAi(HMS00882). Panels to
850 the right, in gray, show single channels, as indicated.
851
852
853 **Figure 1 – figure supplement 3. α-Spec knockdown decreases wing disc thickness.**
854 (A-C) Lateral views of wing discs expressing en-Gal4 UAS-RFP UAS-dcr2 crossed with control
855 (Oregon-R, OR) (A), UAS-kstRNAi(v37075) (B) or UAS-α-specRNAi (C), stained with
856 phalloidin to label F-actin (green), Hoechst to label nuclei (blue) and with the posterior
857 compartment marked by RFP (red) and mounted with 40 µm spacers to avoid compressing the
858 discs. Dashed lines indicate 30 µm from the A/P boundary. Scale bar = 20 µm (D) Quantification
859 of wing imaginal disc thickness determined 30 µm from the A/P boundary in anterior (A) and
860 posterior (P) sides for the different genotypes indicated. Statistical significance was determined
861 by Student's t-test. ns: not significative; **P≤0.01; ***P≤0.001
862
863
864 **Figure 2. Knockdown of β_H-Spec or α-Spec increases junctional Jub levels in wing discs**

865 (A-C) Apical sections of wing discs expressing en-Gal4 UAS-RFP UAS-dcr2 Jub:GFP crossed
866 to control (Oregon-R, OR) (A), UAS-kstRNAi(v37075) (B) or UAS-α-specRNAi (C) stained for
867 E-cad (red/gray) showing the effect on Jub:GFP (green/gray) in the posterior compartment
868 (marked by RFP, blue). Dashed yellow line marks the A/P compartment boundary. Panels to the
869 right, in gray, show single channels, as indicated. Scale bar = 20 μm. (D-F) Heat maps of relative
870 junctional Jub:GFP intensity of wing discs. Levels of Jub:GFP relative to E-cad levels are shown
871 for the different genotypes analyzed. Heat map scale is indicated on the top. Number of wing
872 discs used for analysis: Control (OR), n=9; UAS-kstRNAi, n=8; UAS-α-specRNAi, n=8. (G-H)
873 Quantification of Jub:GFP normalized to E-cadherin (G) or to Jub:GFP mean intensity (H) in
874 posterior cells compared to anterior cells (P/A) in wing discs expressing the indicated constructs,
875 displayed as individual values. Data are shown as mean ± 95% CI. Statistical significance was
876 determined by one-way ANOVA with Dunnett's multiple comparison test relative to the control
877 (Oregon-R): ns: not significant, *P<0.05; **P≤0.01; ***P≤0.001; ****P≤0.0001
878
879
880 **Figure 2 – figure supplement 1. β_H-spec modulates the recruitment of Jub:GFP to AJs.**
881 (A) Third instar wing disc expressing en-Gal4 UAS-dcr2 UAS-RFP (blue) Jub:GFP (green/gray)
882 in combination with UAS-kstRNAi(HMS00882) (A) stained for E-cad (red/gray). Dashed yellow
883 line marks A/P compartment boundary. (B, C) Apical sections of wing discs expressing en-Gal4
884 UAS-RFP UAS-dcr2 Jub:GFP crossed to control (Oregon-R, OR) (B), UAS-kstRNAi(v37075)
885 (C) from Figure 2. Columns to the right show higher magnification views of the Jub:GFP
886 channel anterior (a) and posterior boxes (p).
887
888
889 **Figure 3. Jub is required for β_H-Spec and α-Spec regulation of wing size and ex-lacZ**
890 (A-J) Representative adult wings from flies cultured at 29ºC and expressing UAS transgenes
891 altering spectrin and/or Jub expression under control of a nub-Gal4 (nubG4) driver. (K)
892 Quantification of wing area (mean ± 95% CI) Number of wing discs used for analysis: Control
893 (OR), n=20; UAS-kstRNAi[GD], n=20; UAS-kstRNAi[HMS], n=21; UAS-α-specRNAi, n=20;
894 UAS-jubRNAi, n=20, UAS-jubRNAi UAS-kstRNAi[GD], n=20; UAS-jubRNAi UAS-
895 kstRNAi[HMS], n=20; UAS-jubRNAi UAS-α-specRNAi, n=20; UAS-kstCRISPRa, n=22; UAS-

896 kst[EP], n=26. Statistical significance was determined by a one-way ANOVA with Tukey's
897 multiple comparison test. Statistical comparisons are shown relative to nub-Gal4 UAS-dcr2/+ in
898 green, relative to nub-Gal4 UAS-dcr2 UAS-jubRNAi in purple and relative to UAS-kstRNAi in
899 blue. (L-Q) Third-instar wing discs expressing ex-lacZ en-Gal4 UAS-dcr2 UAS-GFP (green)
900 crossed to OR (L), UAS-kstRNAi (M), UAS-jubRNAi (N), UAS-jubRNAi UAS-kstRNAi (O),
901 UAS-α-specRNAi (P), UAS-jubRNAi UAS-α-specRNAi (Q) stained for expression of ex-lacZ
902 (red/white). Dashed yellow line indicates the A/P compartment boundary.
903
904
905 **Figure 3 - figure supplement 1 *kst* phenotypes are suppressed by reduction of tension**
906 (A-B) Representative adult wings from flies cultured at 29ºC expressing nub-Gal4 and UAS
907 transgenes reducing myosin activity (UAS-rokRNAi) enhancing RNAi (UAS-Dcr2) and in (B)
908 knocking down β_H-Spec (UAS-kstRNAi(v37075)). (C) Quantification of wing area (mean and
909 95% CI, n = 20). Statistical significance was determined by one-way ANOVA with Tukey's
910 multiple comparison test. Statistical comparisons are shown relative to nub-Gal4 UAS-dcr2 (data
911 from Figure 3) in green or between nub-Gal4 UAS-dcr2 UAS-rokRNAi genotypes in black. (D-
912 E) Sections of wing imaginal discs expressing en-Gal4 UAS-rokRNAi UAS-Dcr2 Jub:GFP
913 crossed to control (Oregon-R) (D) or UAS-kstRNAi(v37075) (E) stained for E-cad (red/gray)
914 showing the effect of reducing cytoskeletal tension on Jub:GFP (green/gray) in the posterior
915 compartment (marked by Dcr2 immunostaining, blue). Scale bar = 20 μm.
916
917
918 **Figure 4. β_H-Spec and α-Spec do not co-localize in wing discs.**
919 (A-C) Wing discs expressing Kst:YFP immunostained with α-Spec (red/gray) and E-cad
920 (blue/gray) antibodies showing the localization of β_H-Spec (Kst:YFP, green/gray) and α-Spec at
921 the AJ (A), below the AJ (B) and in cross sections (C). Upper yellow arrow in cross section
922 indicates AJ layer, lower yellow arrow indicates "Below AJ" layer. Inset shows higher
923 magnification of single channels from the boxed region in A. (D,E) Wing discs expressing
924 Kst:GFP (D) or β-spec:GFP (E), with GFP in green and signal from Proximity Ligation Assays
925 (PLA) using rabbit anti-GFP and mouse α-Spec antibodies in magenta.
926

927

928 **Figure 5. Influence of spectrin knockdowns on spectrin subunit localization in wing discs.**
929 (A-C) Apical sections of wing discs expressing en-Gal4 UAS-dcr2 Kst:YFP (green/gray) along
930 with UAS-α-specRNAi (A), UAS-β-specRNAi (B) and UAS-kstRNAi (C) immunostained for α-
931 Spec (A and C, blue/gray) or β-Spec antibodies (B, blue/gray). The AJ layers were obtained by
932 ImSAnE, using as a reference the E-cad channel and 7 layers were projected (2.1 μm). (D,E)
933 Sections of wing discs expressing en-Gal4 UAS-RFP (blue) UAS-dcr2 crossed with UAS-α-
934 specRNAi (D) or UAS-β-specRNAi (E) stained with mouse α-Spec (green/gray) and rabbit β-
935 Spec antibody (red/gray) . Dashed yellow lines indicate the A/P compartment boundary. Scale
936 bar = 20 μm.
937
938

939 **Figure 6. βH-Spec colocalizes with myosin and is regulated by myosin activity**
940 (A,B) Wing disc co-expressing Kst:GFP (green/gray) and the labelled myosin II subunit
941 sqh:mCherry (red/gray) in apical horizontal sections (A) and lateral sections (B), co-stained with
942 phalloidin for F-actin (blue/gray). (C-E) Apical sections of wing discs expressing en-Gal4 UAS-
943 RFP UAS-dcr2 kst:YFP crossed to (Oregon R, OR) (C), UAS-rokRNAi (D) or UAS-sqhEE (E)
944 in the posterior compartment (marked by RFP, blue), showing the effect of altering myosin
945 activity on Kst:YFP. Dashed yellow lines lines mark the A/P compartment boundary. Scale bar =
946 20 μm. (F) Higher magnification of the boxed regions indicated in E. Scale bar = 10 μm (G-I)
947 Heat maps of junctional Kst:YFP intensity relative to E-cad in en-Gal4 UAS-RFP UAS-dcr2
948 kst:YFP crossed to (Oregon R, OR) (C), UAS-rokRNAi (D) or UAS-sqhEE (E) wing discs (n=5
949 for each genotype), as in the representative examples shown in C to E. Heat map scale is at
950 bottom. (J) Quantification of Kst:YFP intensity normalized to E-cadherin in posterior cells (P)
951 compared to anterior cells (A) in wing discs expressing the indicated constructs under en-Gal4
952 control (n=5). Data are shown as mean ± 95% CI, error bars indicate CI. Statistical significance
953 was determined by a one-way ANOVA with Dunnett's multiple comparison test relative to the
954 control (Oregon-R): ns: not significant, *$P<0.05$; **$P\leq0.01$.
955
956

957 **Figure 6- figure supplement 1. Additional analysis of β_H-Spec localization and the effect of**
958 **changes in tension on myosin.**
959 (A) Lateral view of a wing imaginal disc co-expressing Kst:GFP (green) and the labelled myosin
960 II subunit sqh:mCherry (magenta) stained with α-Spec antibody (blue). Scale bar = 10 μm (B)
961 Linescan along the yellow line in A showing the intensities of Kst:GFP (green), Sqh::mCherry
962 (magenta) and α-Spec. (C) Apical sections of a wing disc expressing en-Gal4 UAS-RFP UAS-
963 dcr2 sqh:GFP crossed to UAS-rokRNAi in the posterior compartment (marked by Dcr2
964 immunostaining, blue), showing the effect of decreasing myosin activity on Sqh:GFP
965 (green/gray). (D) Apical sections of a wing disc expressing en-Gal4 UAS-dcr2 zip:GFP (myosin
966 heavy chain subunit tagged with GFP) crossed to UAS-sqh^{EE} in the posterior compartment
967 (marked by RFP, blue), showing the effect of increasing myosin activity on Zip:GFP
968 (green/gray). Discs were also stained for E-cad (red/gray). As described previously (Rauskolb et
969 al., 2014), decreasing myosin activity decreases myosin levels near apical junctions and
970 increasing myosin activity increases myosin levels near apical junctions. Scale bar = 20 μm.
971
972
973 **Figure 7. β_H-Spec overexpression reduces in junctional tension in wing discs.**
974 (A-B) Apical sections of wing imaginal discs expressing en-Gal4 UAS-RFP UAS-dcr2 sqh:GFP
975 (A) or en-Gal4 UAS-RFP UAS-dcr2 jub:GFP (B) crossed to UAS-kst-CRISPRa showing the
976 effect on Sqh:GFP or Jub:GFP levels and localization in the posterior compartment (marked by
977 RFP, blue). Yellow dashed line indicates the A/P compartment boundary. Scale bar = 20 μm; all
978 images are at the same magnification. (C-D) Heat maps of relative junctional Sqh:GFP (C) or
979 Jub:GFP (D) intensity of wing discs. Levels of Sqh:GFP relative to E-cad levels are shown for
980 the different genotypes analyzed in A-B. Heat map scale is indicated on the top. Number of wing
981 discs used for analysis: UAS-kst-CRISPRa with Sqh:GFP, n=5; UAS-kst-CRISPRa with
982 Jub:GFP, n= 6 (E-F) Quantification of Sqh:GFP overlapping E-cad in posterior cells (P)
983 compared to anterior cells (A) in wing disc expressing the indicated constructs, displayed as
984 individual values, normalized by E-cad (E) or normalized by the mean intensity of Sqh:GFP (F).
985 (G-H) Quantification of Jub:GFP overlapping E-cad in posterior cells (P) compared to anterior
986 cells (A) in wing disc expressing the indicated constructs, displayed as individual values,
987 normalized by E-cad (G) or normalized by the mean intensity of Jub:GFP (H). (I) Average recoil

988 velocities after laser cutting of cell junctions in anterior (A) or posterior (P) compartments of
989 wing discs expressing UAS-kstCRISPRa in posterior cells (n=20). Data are shown as mean ±
990 95% CI. Statistical significance in (I) was determined by Student's t-test between A and P. For
991 (J) and (K), statistical significance was determined by a one-way ANOVA with Dunnett's
992 multiple comparison test relative to the control (Oregon-R): ns: not significant, *P<0.05;
993 **P≤0.01; ***P≤0.001; ****P≤0.0001.
994
995
996 **Figure 7 - figure supplement 1.**
997 (A) Apical sections of a wing imaginal disc expressing en-Gal4 tubG80ts kst:GFP crossed with
998 UAS-kstCRISPRa, stained for E-cad (magenta). Expression of Kst:GFP (green) was induced by
999 transferring the flies from 18ºC to 29ºC for 24 h. (B) Western blots of wing disc lysates with the
1000 genotypes shown in the figure: nub-Gal4 UAS-Dcr2 kst:GFP crossed with w^{1118} (control) and
1001 UAS-kstCRISPRa (experimental). Kst:GFP was detected using a GFP antibody. GAPDH was
1002 used as a loading control. (C) Third instar wing imaginal discs expressing enGal4 UAS-dcr2
1003 UAS-RFP sqh:GFP in combination with UAS-kstP[EPgy2]EY01010. (D) Third instar wing
1004 imaginal discs expressing enGal4 UAS-dcr2 UAS-RFP jub:GFP in combination with UAS-
1005 kstP[EPgy2]
1006 EY01010.
1007
1008
1009 **Figure 8. β_H-Spec and myosin have overlapping binding sites on F-actin.**
1010 (A-C) Co-sedimentation assays with βH-Spec CH domains (Spectrin), F-actin, and myosin-II
1011 subfragment-1-like protein (myosin). For all sedimentation assays, A, M, Sp, E, and R refer to F-
1012 actin, myosin heavy chain, spectrin, myosin essential light chain and myosin regulatory light
1013 chain, respectively. Mw indicates marker and S and P refer to supernatant and pellet,
1014 respectively. Quantification shows mean ± S.D. of the sedimentation behavior of spectrin and
1015 myosin with F-actin (n = 3). (A) Co-sedimentation assay between spectrin (0-12 μM) and F-actin
1016 (2 μM). (B) Co-sedimentation assay between myosin (0-2.59 μM) and F-actin (2 μM). (C) Co-
1017 sedimentation assay between spectrin (12 μM), myosin (0-2.59 μM) and F-actin (2 μM).
1018 Quantification shows that myosin reduces spectrin binding by ~50% (bottom panel). (D-D'')

1019 Model of the *Drosophila* CH1 domain (yellow) bound to F-actin (grey) (D). Model of the
1020 *Drosophila* myosin motor domain (purple) bound to F-actin (grey) (D'). Superimposition of the
1021 CH1 and myosin motor domain on F-actin. The two strands of the actin filament are shown in
1022 light and dark grey and subdomains are indicated.
1023
1024
1025 **Figure 8 – figure supplement 1. Additional examination of competition between β_H-Spec**
1026 **and myosin for F-actin.**
1027 (A) Quantification of the binding behavior of myosin to F-actin in the presence and absence of
1028 spectrin in co-sedimentation assays. The similarity in actin binding indicates that pre-loading
1029 spectrin does not interfere with myosin binding to F-actin under these assay conditions. (B)
1030 Model of the *Drosophila* CH1-CH2 domain (CH1, yellow; CH2, blue) bound to F-actin (grey)
1031 (B'). Model of the *Drosophila* myosin motor domain (purple) bound to F-actin (grey) (B'').
1032 Superimposition of the CH1-CH2 and myosin motor domain on F-actin. The two strands of the
1033 actin filament are shown in light and dark grey and subdomains are indicated.

Figure 1, Ibar et al

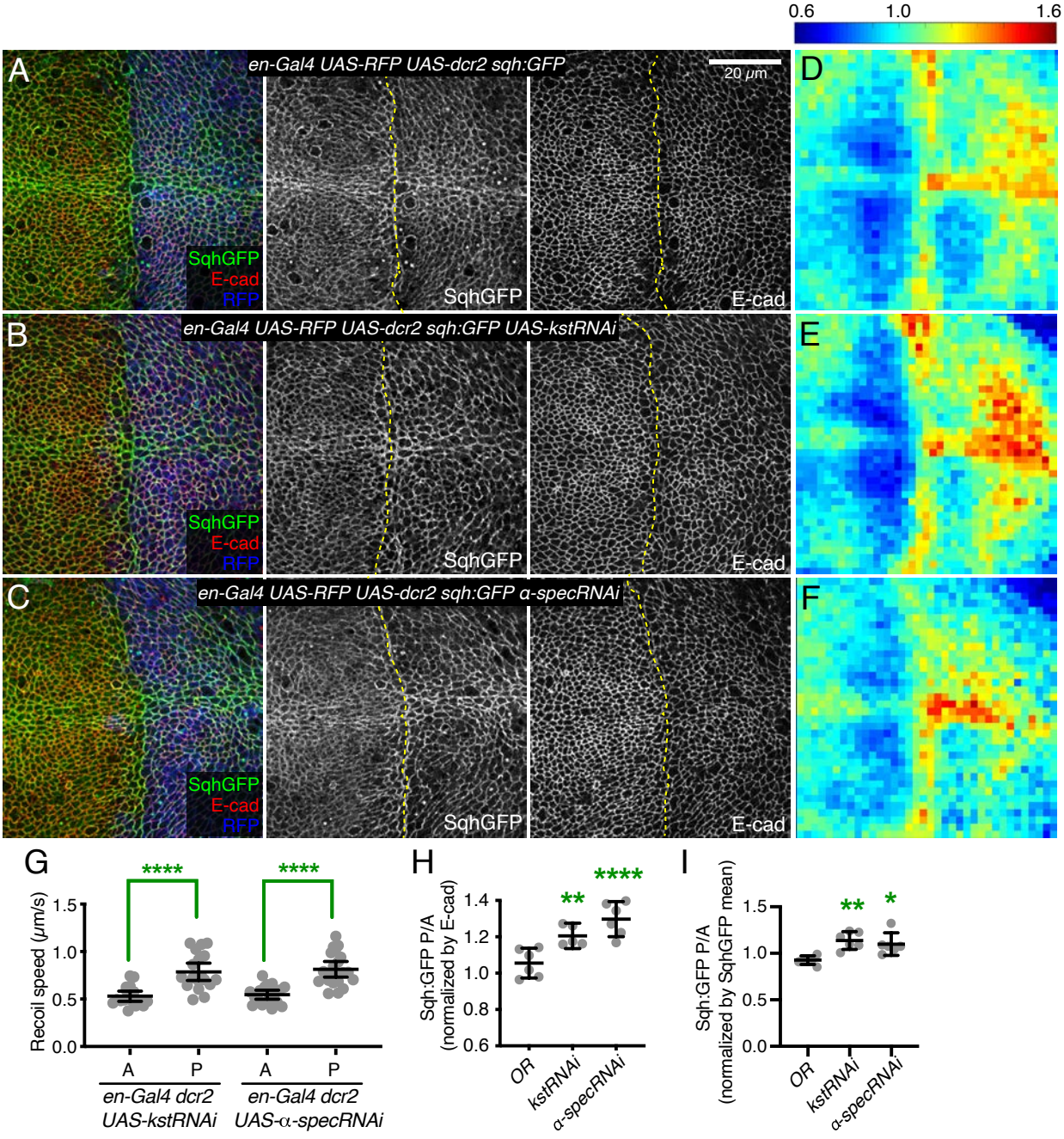

Figure 1-supplement 1, Ibar et al

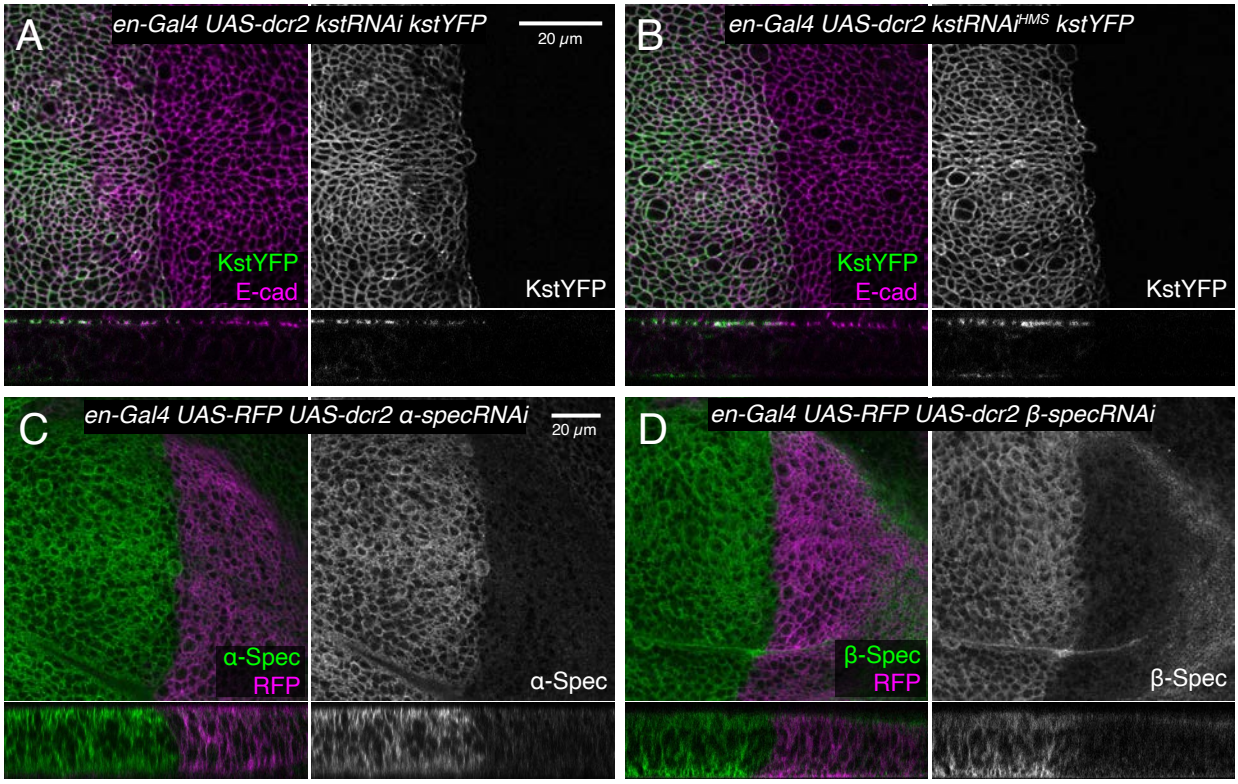

Figure 1-supplement 2, Ibar et al

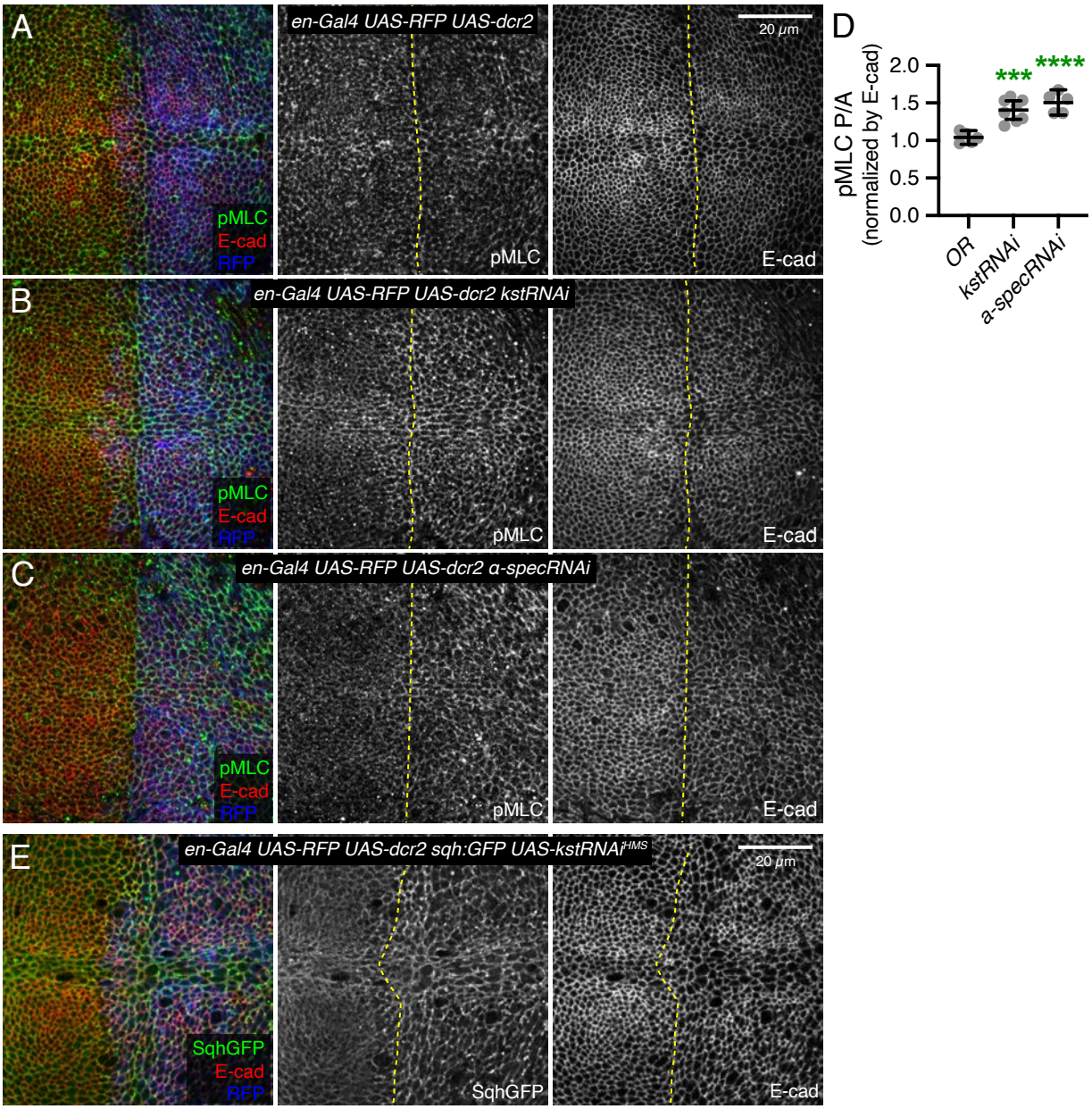

Figure 1-supplement 3, Ibar et al

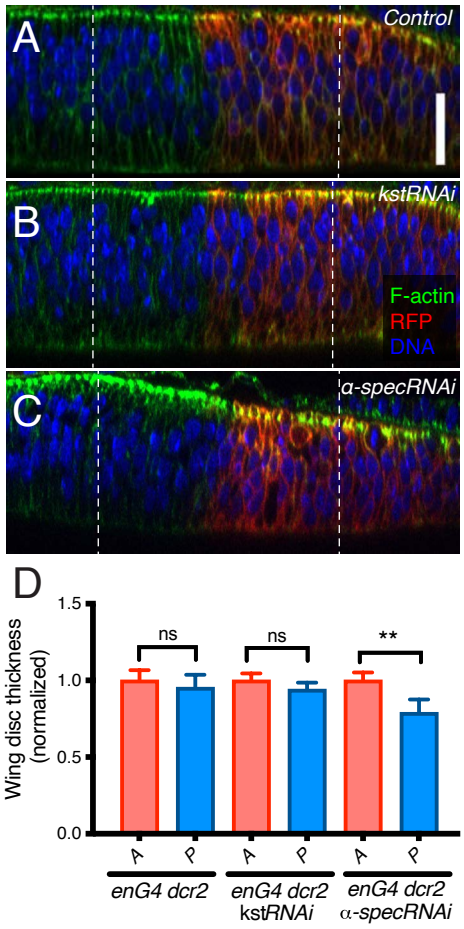

Figure 2, Ibar et al

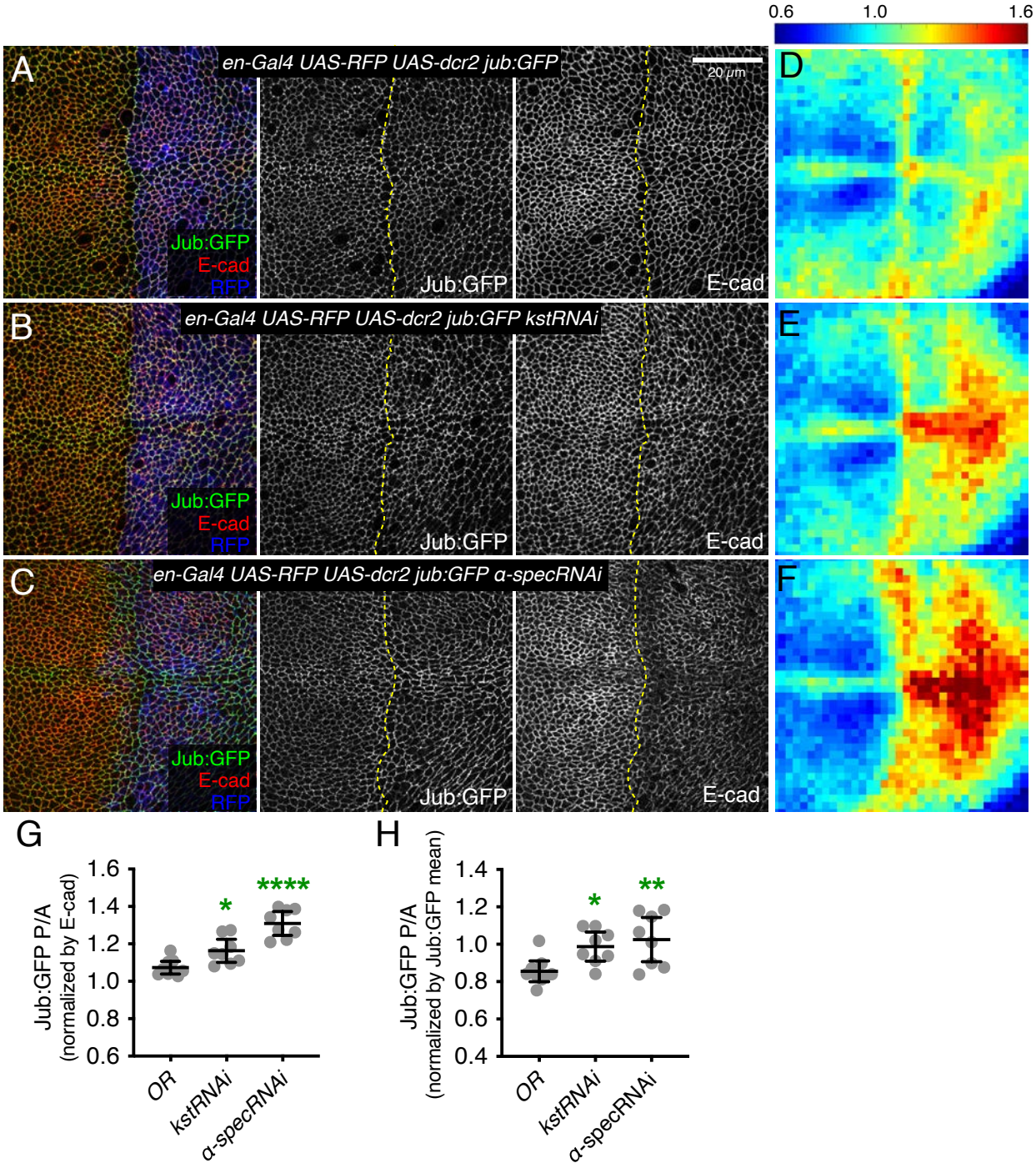

Figure 2-supplement 1, Ibar et al

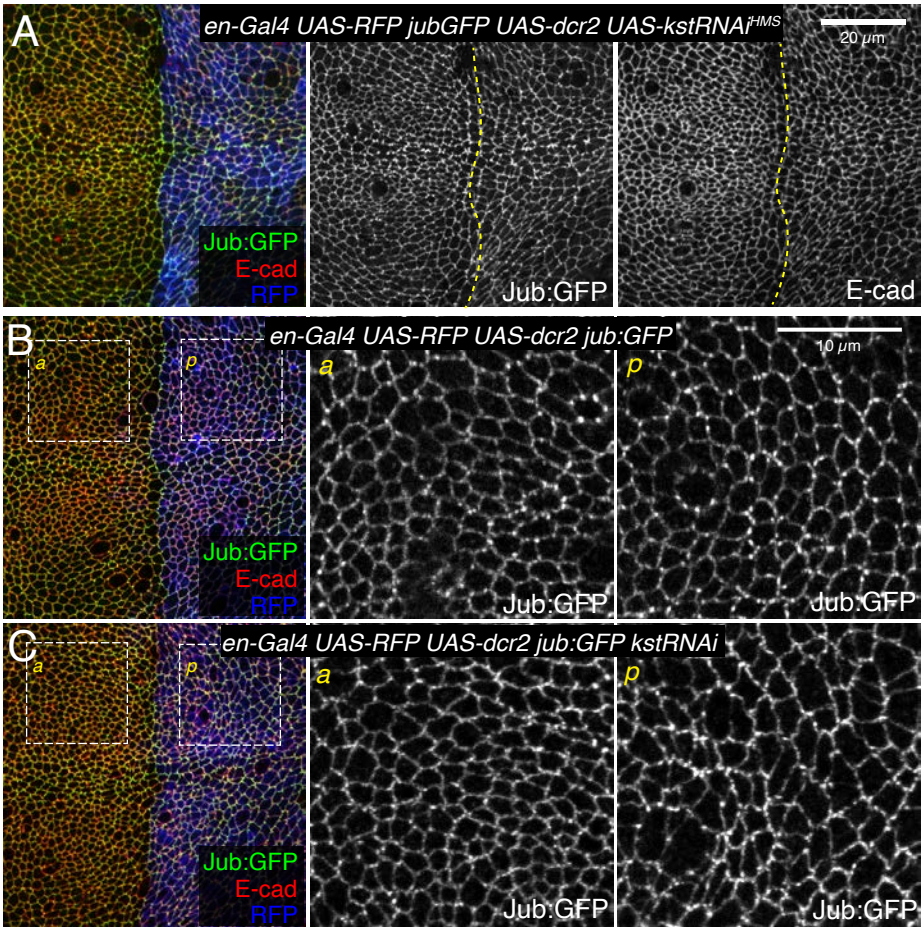

Figure 3, Ibar et al

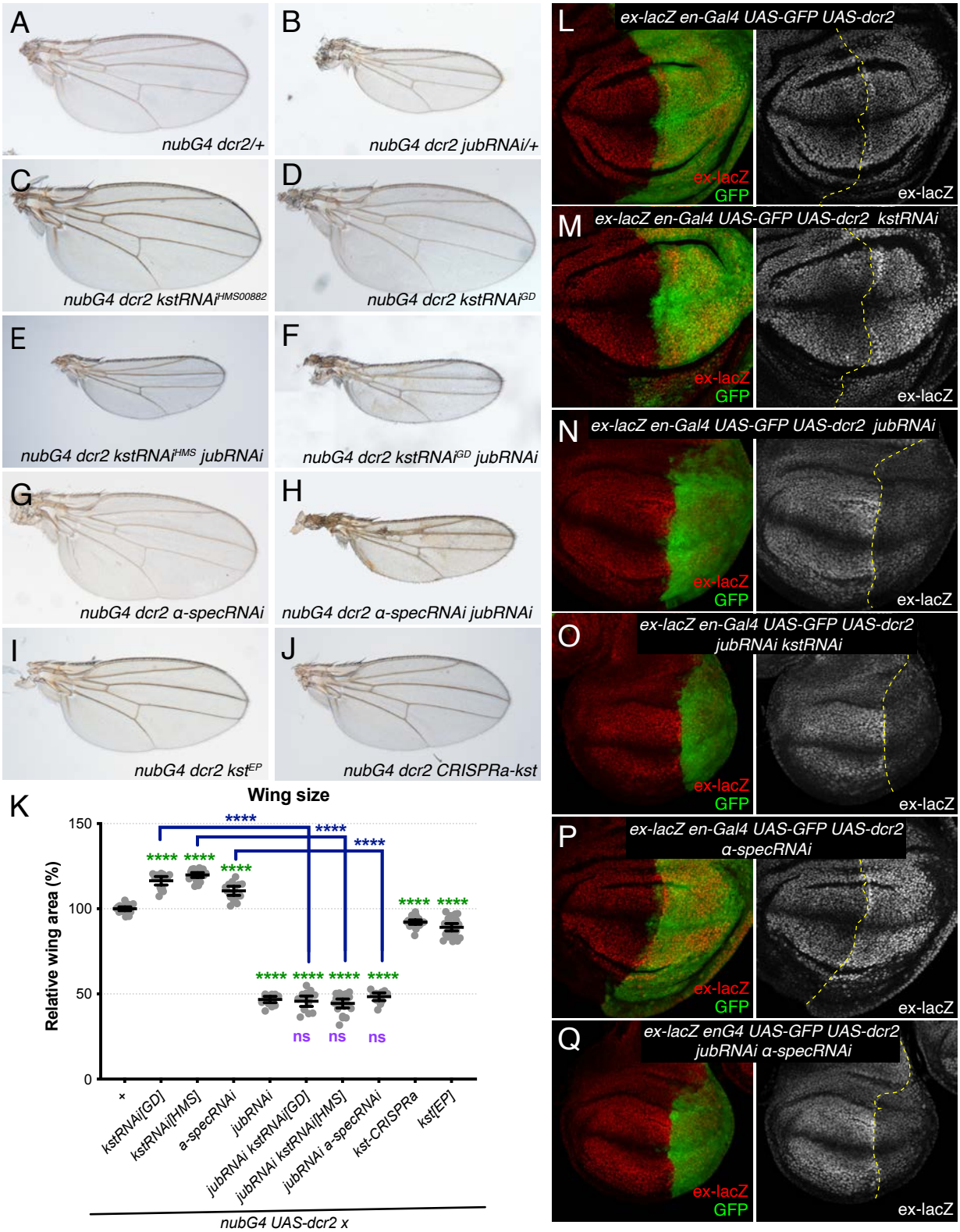

Figure 3-supplement 1, Ibar et al

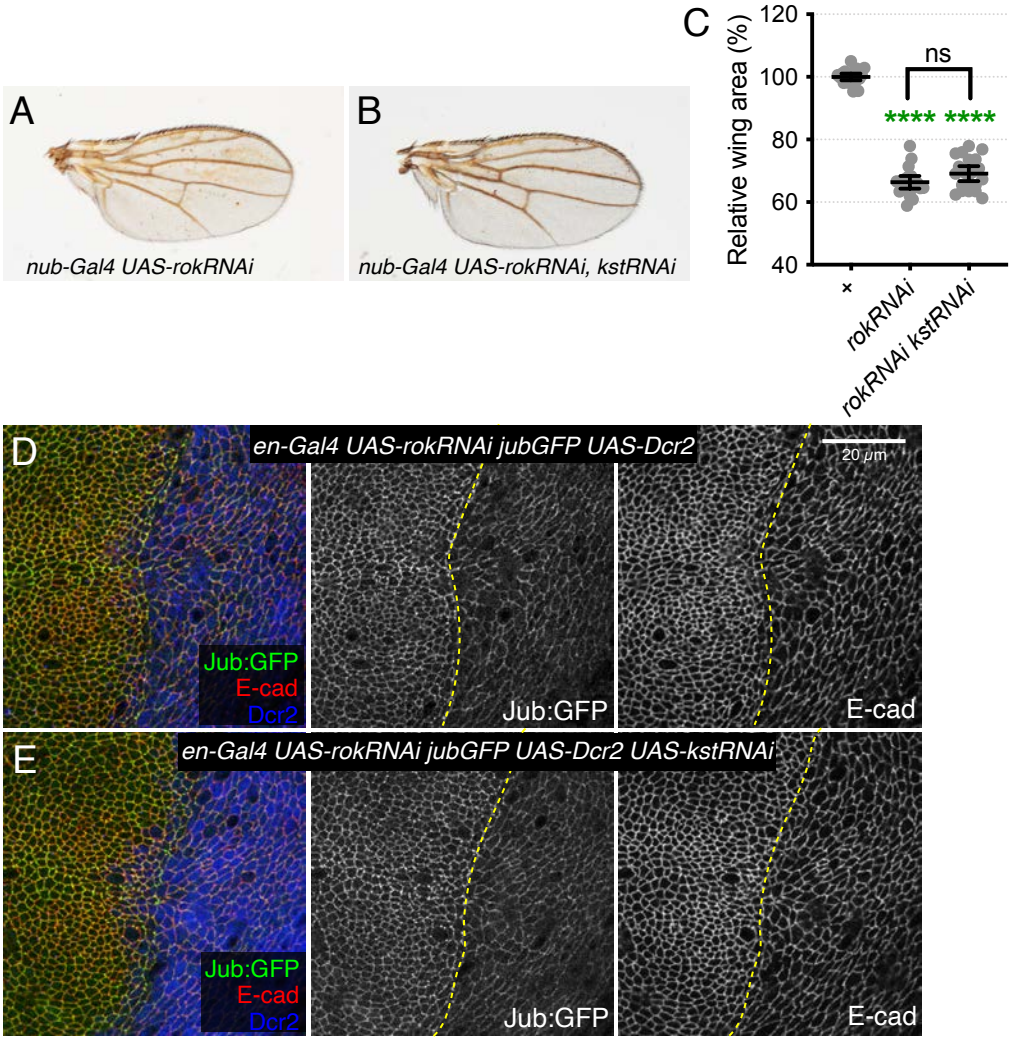

Figure 4, Ibar et al

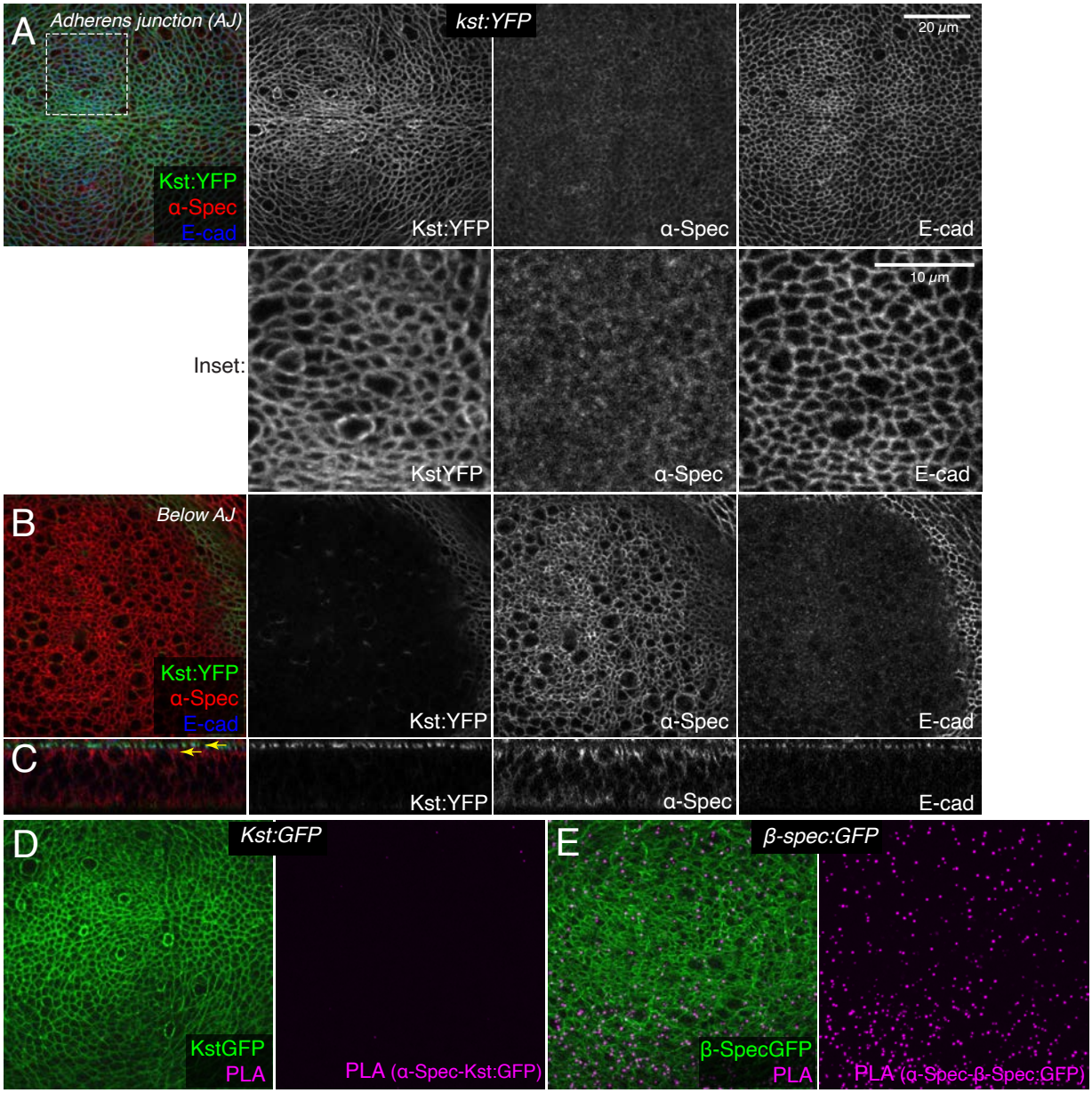

Figure 5, Ibar et al

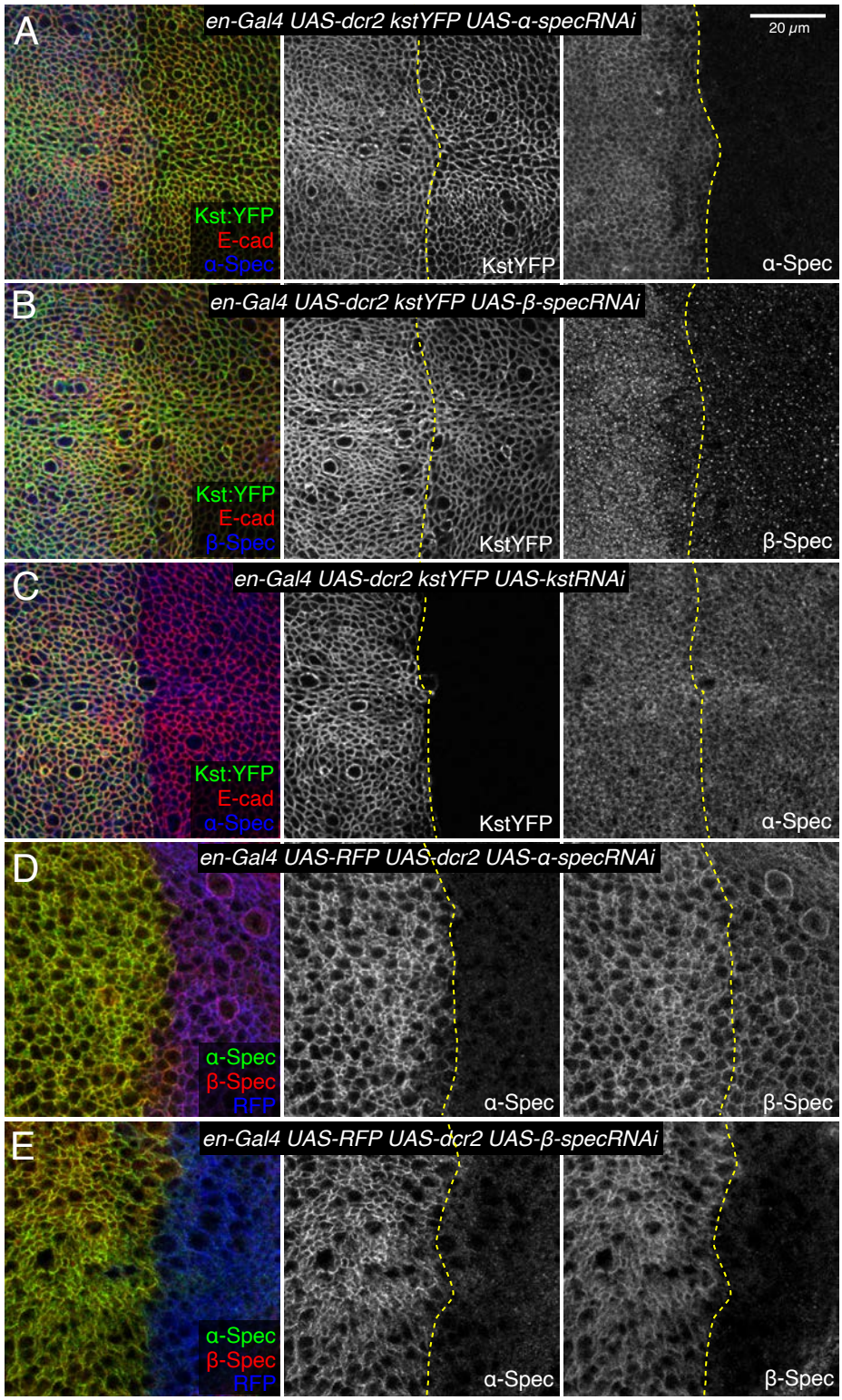

Figure 6, Ibar et al

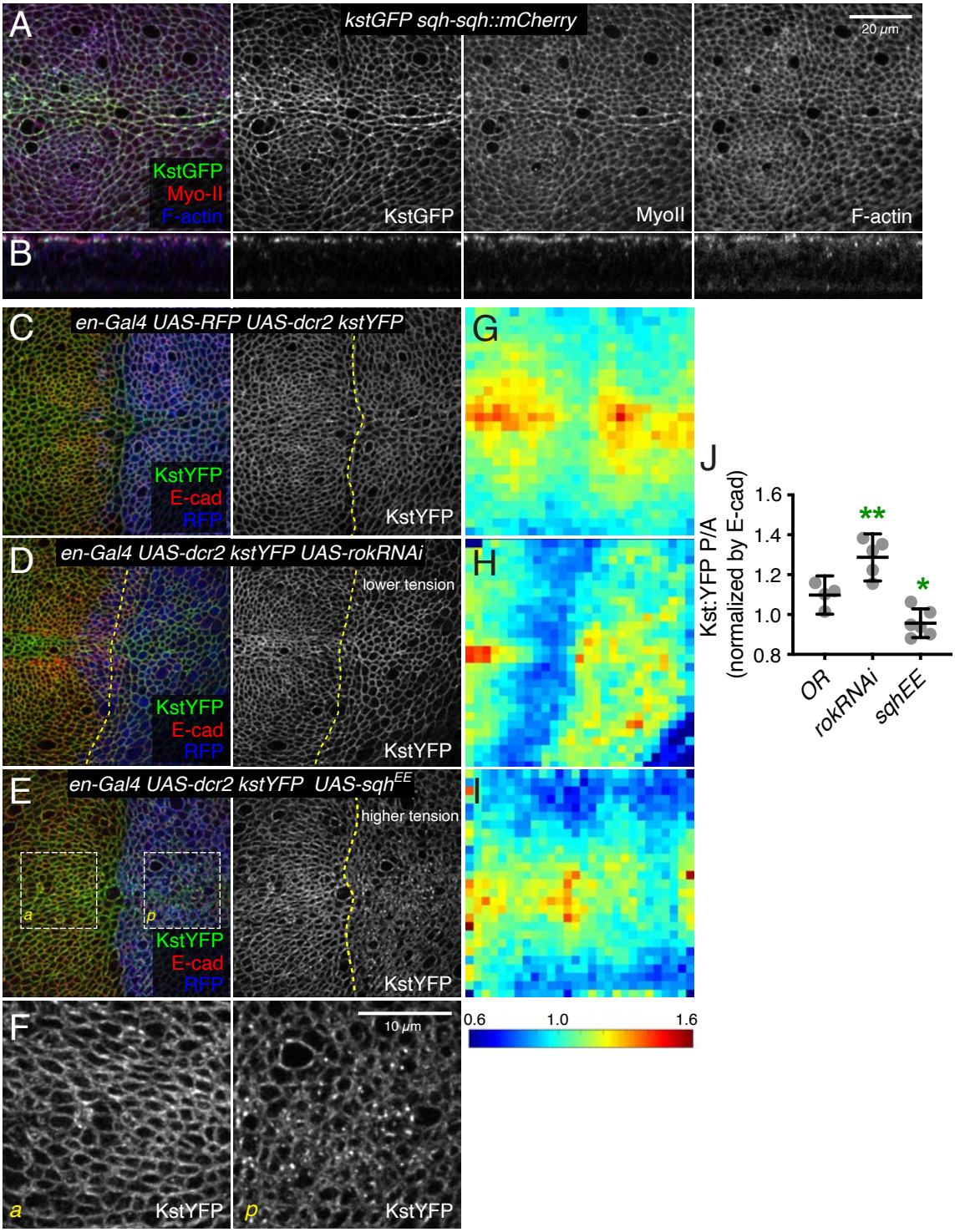

Figure 6-supplement 1, Ibar et al

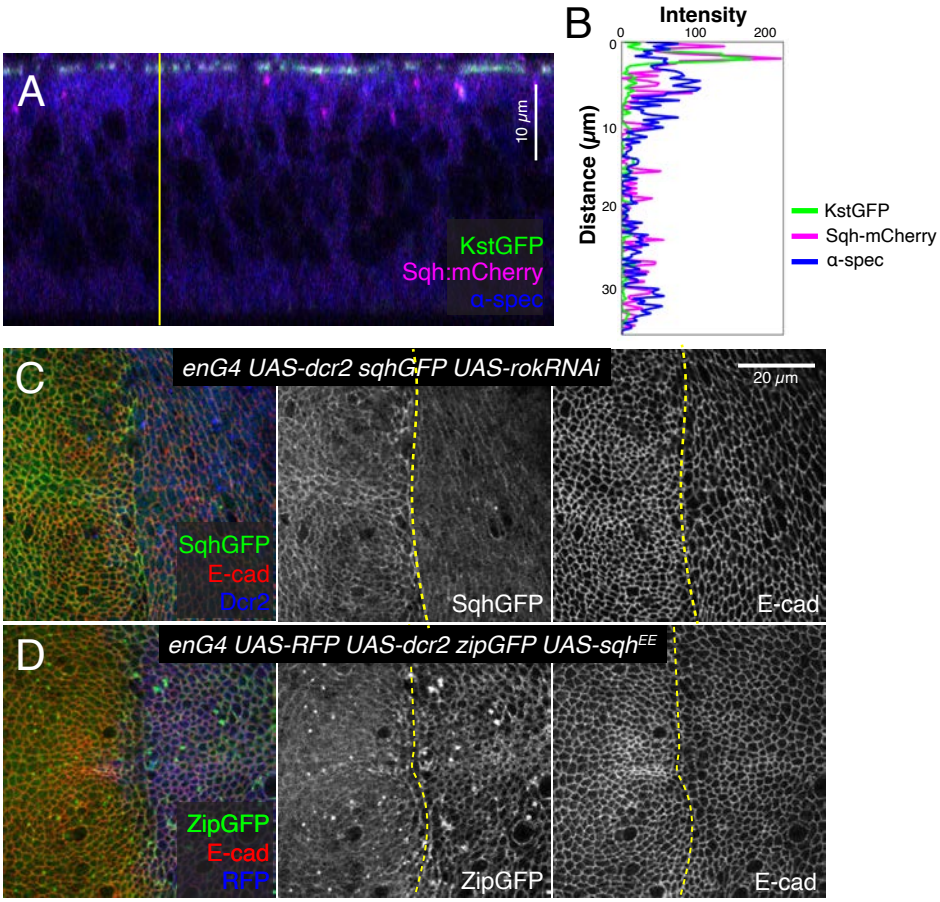

Figure 7, Ibar et al

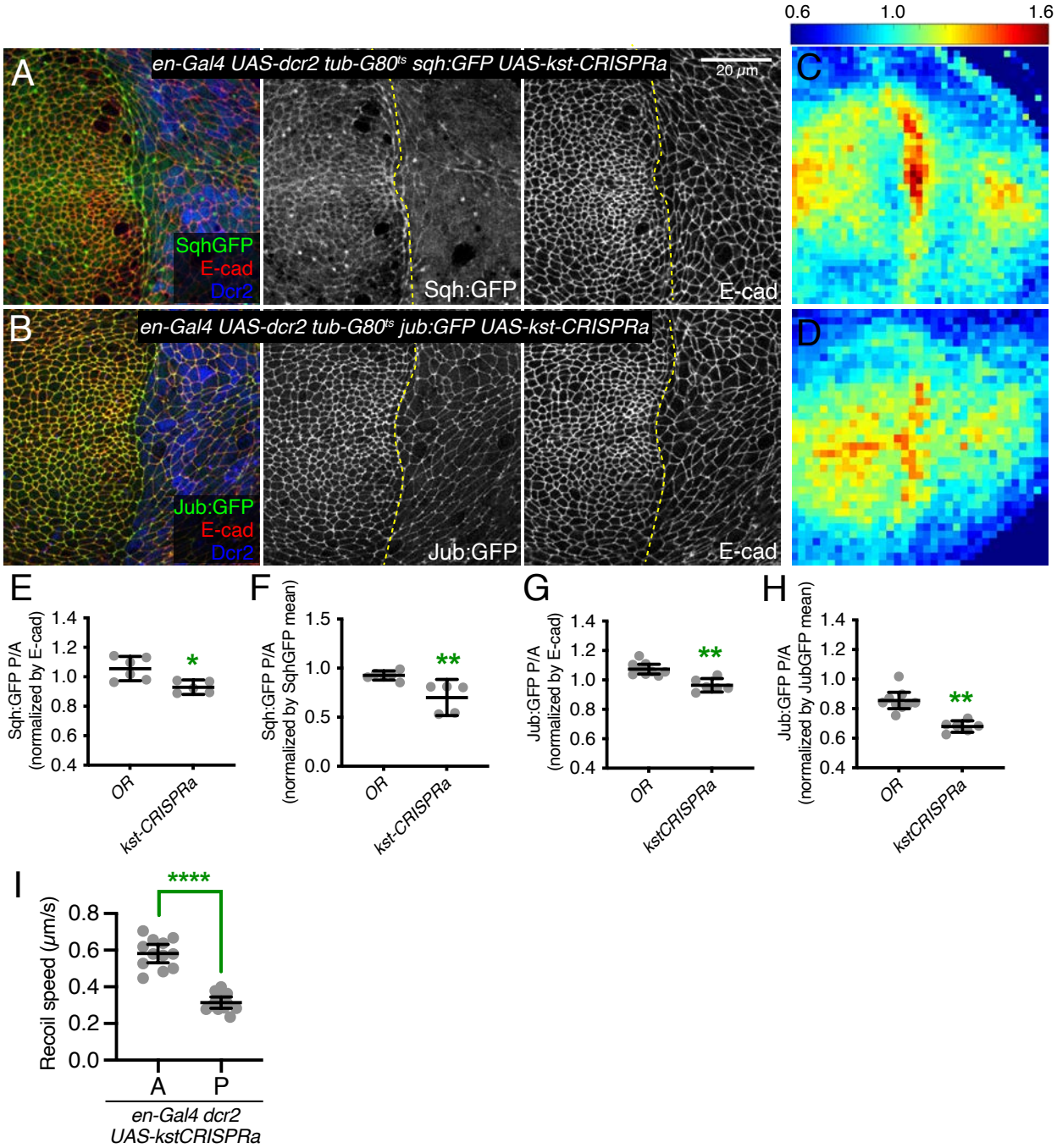

Figure 7-supplement 1, Ibar et al

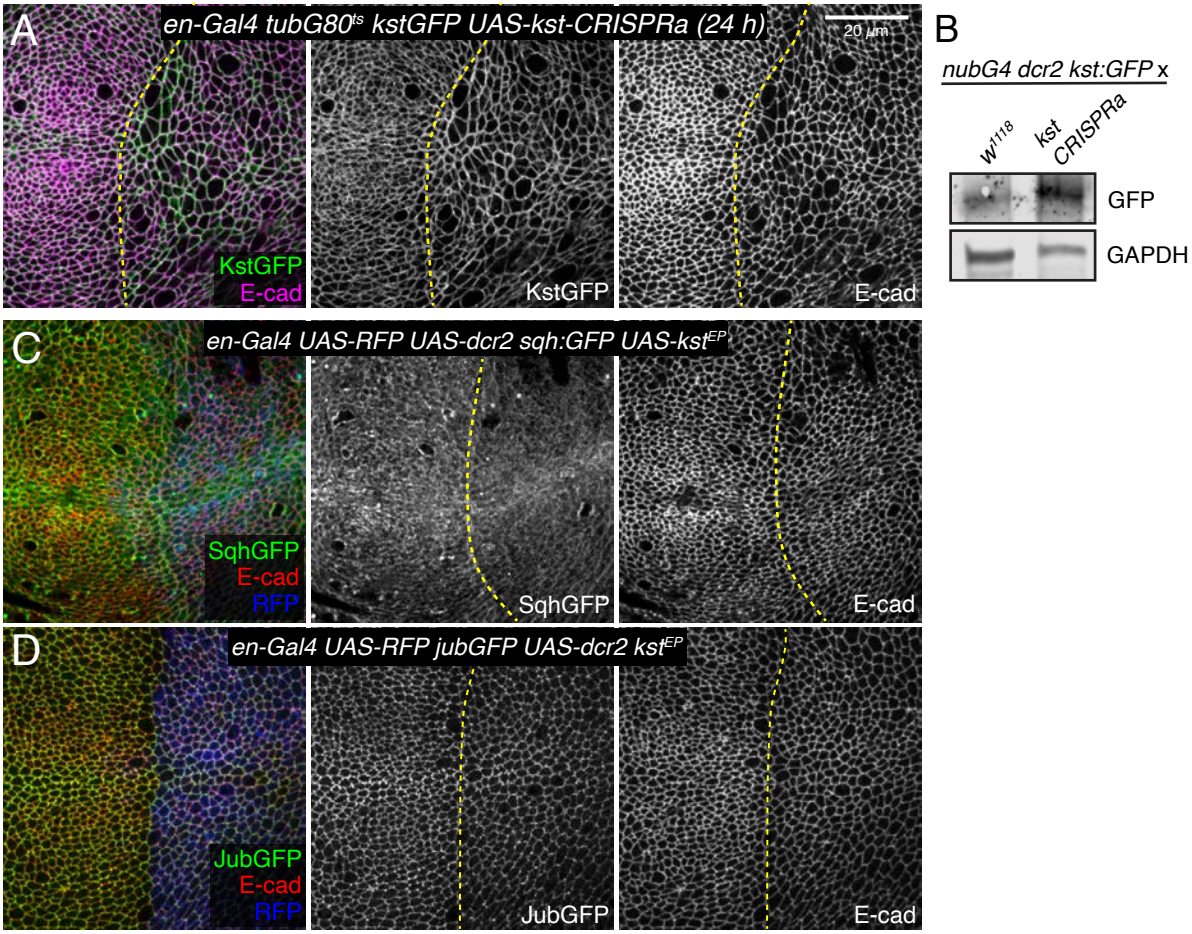

Figure 8, Ibar et al

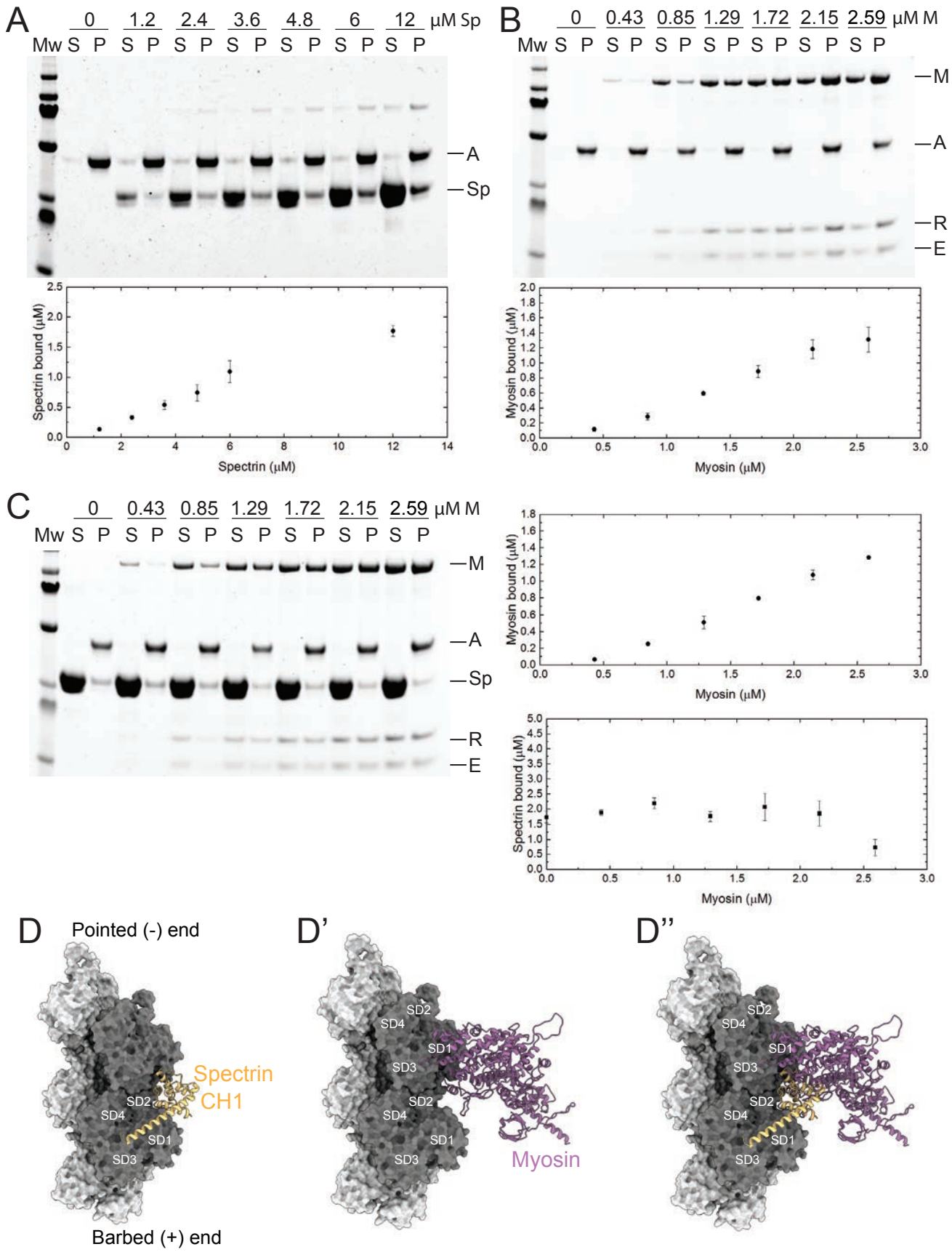
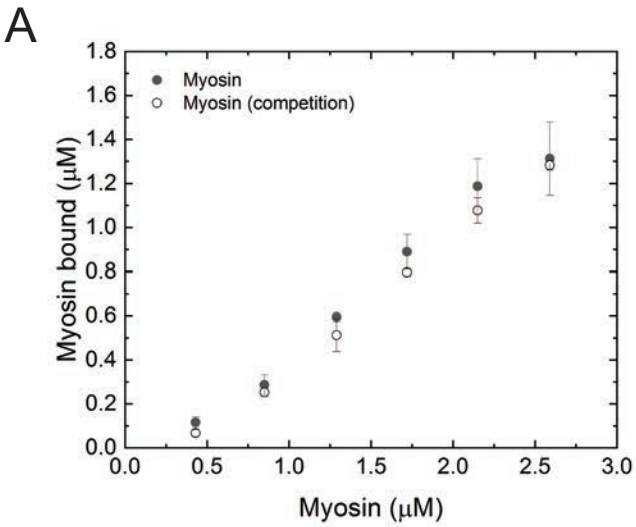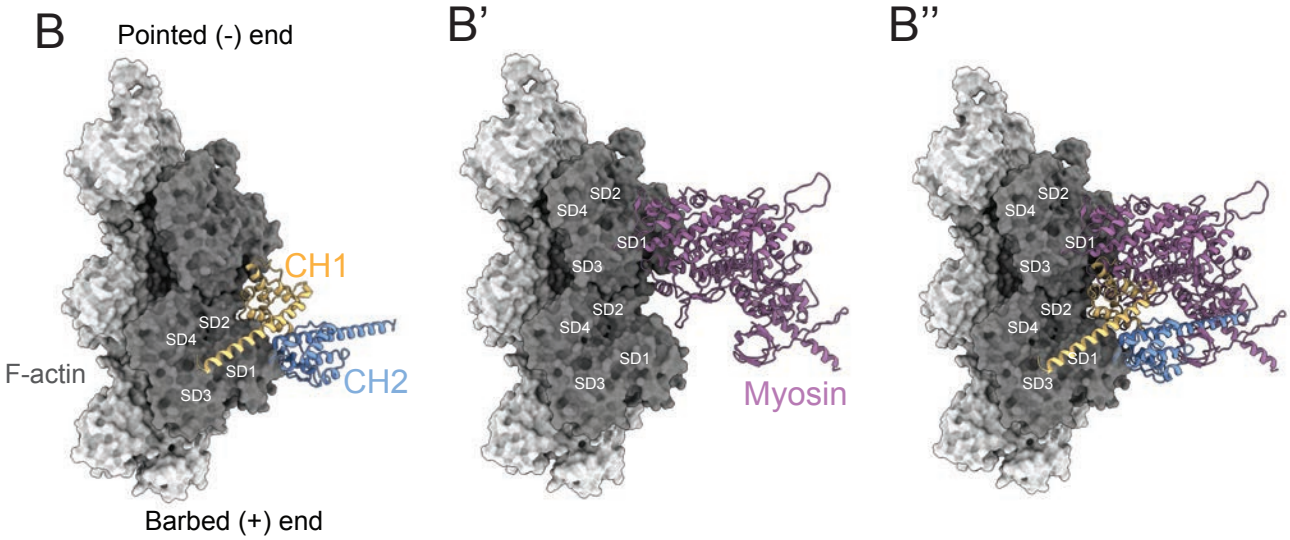
Figure 8-supplement 1, Ibar et al